

RESEARCH ARTICLE

10.1029/2018JC014568

Special Section:

The Arctic: An AGU Joint
Special Collection

Key Points:

- We evaluate biological carbon cycling in the Pacific Arctic during the late open water season
- $\Delta O_2/Ar$ and ΔpCO_2 observations suggest an important role for late season biological activity toward maintaining an ocean carbon sink
- High mesoscale variability in biological metabolism inferred from O_2/Ar suggests localized and likely episodic nutrient supply

Supporting Information:

- Supporting Information S1
- Movie S1
- Movie S2
- Movie S3
- Movie S4
- Movie S5
- Movie S6

Correspondence to:

L. Juranek,
ljuranek@coas.oregonstate.edu

Citation:

Juranek, L., Takahashi, T., Mathis, J., & Pickart, R. (2019). Significant biologically mediated CO_2 uptake in the Pacific Arctic during the late open water season. *Journal of Geophysical Research: Oceans*, 124, 821–843. <https://doi.org/10.1029/2018JC014568>

Received 17 SEP 2018

Accepted 7 JAN 2019

Accepted article online 10 JAN 2019

Published online 1 FEB 2019

Significant Biologically Mediated CO_2 Uptake in the Pacific Arctic During the Late Open Water Season

L. Juranek¹ , T. Takahashi² , J. Mathis³ , and R. Pickart⁴ 

¹College of Earth, Ocean, and Atmospheric Sciences, Oregon State University, Corvallis, OR, USA, ²Lamont-Doherty Earth Observatory, Columbia University, Palisades, NY, USA, ³NOAA Arctic Research Program, Silver Spring, MD, USA, ⁴Woods Hole Oceanographic Institution, Woods Hole, MA, USA

Abstract Shifting baselines in the Arctic atmosphere-sea ice-ocean system have significant potential to alter biogeochemical cycling and ecosystem dynamics. In particular, the impact of increased open water duration on lower trophic level productivity and biological CO_2 sequestration is poorly understood. Using high-resolution observations of surface seawater dissolved O_2/Ar and pCO_2 collected in the Pacific Arctic in October 2011 and 2012, we evaluate spatial variability in biological metabolic status (autotrophy vs heterotrophy) as constrained by O_2/Ar saturation ($\Delta O_2/Ar$) as well as the relationship between net biological production and the sea-air gradient of pCO_2 (ΔpCO_2). We find a robust relationship between ΔpCO_2 and $\Delta O_2/Ar$ (correlation coefficient of -0.74 and -0.61 for 2011 and 2012, respectively), which suggests that biological production in the late open water season is an important determinant of the air-sea CO_2 gradient at a timeframe of maximal ocean uptake for CO_2 in this region. Patchiness in biological production as indicated by $\Delta O_2/Ar$ suggests spatially variable nutrient supply mechanisms supporting late season growth amidst a generally strongly stratified and nutrient-limited condition.

Plain Language Summary The Arctic is experiencing rapid change. One of the most notable changes is an increase in the length of time coastal areas of the Arctic are ice-free in summer, which may affect the growth patterns of microscopic marine plants at the bottom of the food chain in Arctic ecosystems. We investigate how the growth at the base of the food chain is responding to these sea ice changes in the late, “open water” period. To track growth, we measure the oxygen content of the surface ocean, which constrains the balance of growth and loss as marine plants photosynthesize and then are consumed and decomposed. We also relate the spatial patterns of net growth to the amount of carbon dioxide (CO_2) gas dissolved in the surface ocean to evaluate the potential impact of biological activity on the uptake of this important greenhouse gas into the surface ocean. We find a surprising relationship between growth and areas of CO_2 uptake by the ocean. This finding is important because it suggests that the biological community facilitates carbon dioxide uptake during a timeframe when previously growth would be inhibited by ice cover.

1. Introduction

The Arctic Ocean is presently undergoing rapid and significant transition in response to climate forcing, with a well-documented decline in sea ice extent, reduction in the average ice thickness, and an increase in open water duration (e.g., Barnhart et al., 2016; Kwok & Rothrock, 2009; Overland & Wang, 2013). An increase in the seasonal sea ice melt, coupled with trends in terrestrial freshwater inputs, has increased upper ocean freshwater content, increasing stratification and potentially impacting exchange of heat and carbon between ocean and atmosphere (e.g., Carmack et al., 2016). These physical system changes will undoubtedly have important consequences for biogeochemical cycling and ecosystem functioning in the Arctic; however, the magnitude and direction of change is currently difficult to predict among multiple confounding responses to individual trends. For example, lower trophic level primary productivity (PP) is predicted to increase in response to declining sea ice extent as a longer open water season and enhanced penetration of light through thinner ice reduces light limitations on growth (Arrigo et al., 2008; Arrigo & van Dijken, 2015; Pabi et al., 2008). However, observations of increasing cloudiness associated with larger open water area would temper these increases (Bélanger et al., 2013). Moreover, reductions in light limitation will not increase PP in regions already limited by availability of inorganic nitrogen, as is

typically the case in the Pacific sector of the Arctic by early August. Therefore, changes in nutrient supply, whether by remote, large-scale forcing or more local, episodic forcing, are required to utilize an extended growing season and drive shifts in PP (e.g., Grebmeier et al., 2015; Tremblay et al., 2015).

With respect to shifting biogeochemistry and ecology, shoulder seasons flanking the short Arctic summer are of particular interest. These transitional windows are occurring earlier/later (Grebmeier et al., 2015) presenting opportunities for spatial and temporal mismatches between growth of primary producers and higher trophic levels, and likely impacting vertical or lateral export characteristics of biogeochemically relevant variables. For example, an earlier spring ice retreat bloom and faster transition from ice-covered to open water conditions may influence grazing and vertical carbon export to benthic communities on Arctic shelves (e.g., Grebmeier et al., 2006, Kahru et al., 2011; Wassmann & Reigstad, 2011). Potential shifts in the late summer shoulder season (September–October) may also be significant: A delayed freeze-up allows passing low-pressure storm systems to impart momentum to the still ice-free, shallow Arctic shelves, potentially enhancing mixing and the supply of “new” nutrients to otherwise depleted surface waters (Wassmann & Reigstad, 2011). This local, episodic supply of nutrients can increase annual PP and allow surface phytoplankton communities to capitalize on the extended growing season over which light is not limiting.

Several recent studies have indicated a role for storms in fueling late open water season biological productivity. A pan-Arctic analysis of phytoplankton bloom phenology from satellite-derived chlorophyll suggested an increased occurrence of fall blooms, with particularly notable changes in the Pacific Arctic sector (i.e., >30% increase in 2007–2012 vs 1998–2001 for the Chukchi Sea), attributed to an increased frequency of storms over the same period (Ardyna et al., 2014). In a separate study, high-frequency microstructure profiling and water sampling at a fixed location (Eulerian observatory) in the northern Chukchi Sea indicated significant increases in upper ocean kinetic energy dissipation rate and upward nutrient flux following three separate storm events with wind speed >10 m/s in September 2013 (Nishino et al., 2015). Finally, Pickart et al. (2013) showed an increased frequency of storm events likely to drive coastal upwelling in the vicinity of Barrow Canyon (Figure 1) in recent decades (1991–2010) based on evaluation of a 70-year weather station record from Barrow, AK (United States). Their analysis suggested that (1) storms occurred more frequently in spring (May) and fall (September–November) because of interactions between the strength/position of the Beaufort High and Aleutian Low atmospheric pressure centers and 2) vertical nitrate supply associated with these events could fuel PP equivalent to 25–50% annual PP estimates based on ^{14}C -incubations (Hill & Cota, 2005).

The impact of these physical and ecological changes on the trajectory of air-sea CO_2 uptake in the Arctic is presently uncertain, and importantly, trajectories of Arctic shelves and deep basins may differ markedly. Cold, highly productive Arctic shelves are predisposed to efficient seasonal sequestration of CO_2 (Bates & Mathis, 2009; Takahashi et al., 2014), and some regional ocean models suggest an increase in continental shelf biological pump activity over an extended growing season can offset sink reductions driven by warming surface temperatures (Manizza et al., 2013). However, observational evidence suggests warming and enhanced stratification (which acts to depress biological carbon sequestration) is already reducing the sink in the deep Beaufort basin of the Western Arctic (Cai et al., 2010; Else et al., 2013). While significant improvements in coverage of air-sea CO_2 flux are allowing refinements in Arctic CO_2 uptake estimates (Evans et al., 2015), separation of CO_2 uptake into abiotic and biotic drivers is difficult owing to the slow equilibration time scale for CO_2 in the upper ocean, and biological rate measurements that impact oceanic CO_2 concentrations over short time scales but are poorly distributed in space and time. Coupled measurements of biological rate terms and air-sea CO_2 fluxes are exceedingly rare. This hinders efforts to evaluate future trajectories of air-sea CO_2 flux and ground-truth the predictions of remote-sensing PP algorithms and ecosystem models.

Here we utilize high-resolution observations of dissolved gases (O_2 , Ar, and $p\text{CO}_2$) to evaluate net biological productivity and investigate biological control of air-sea CO_2 flux in the Pacific Arctic sector in the late open water shoulder seasons of October 2011 and 2012. Our data provide unprecedented detail on the spatial variability of biological production throughout the Pacific Arctic region, allowing us to evaluate mechanisms contributing to observed patterns. We also find a robust association between late season production rates and the air-sea $p\text{CO}_2$ gradient which suggests an important role for biologically mediated CO_2 uptake during the late open water season.

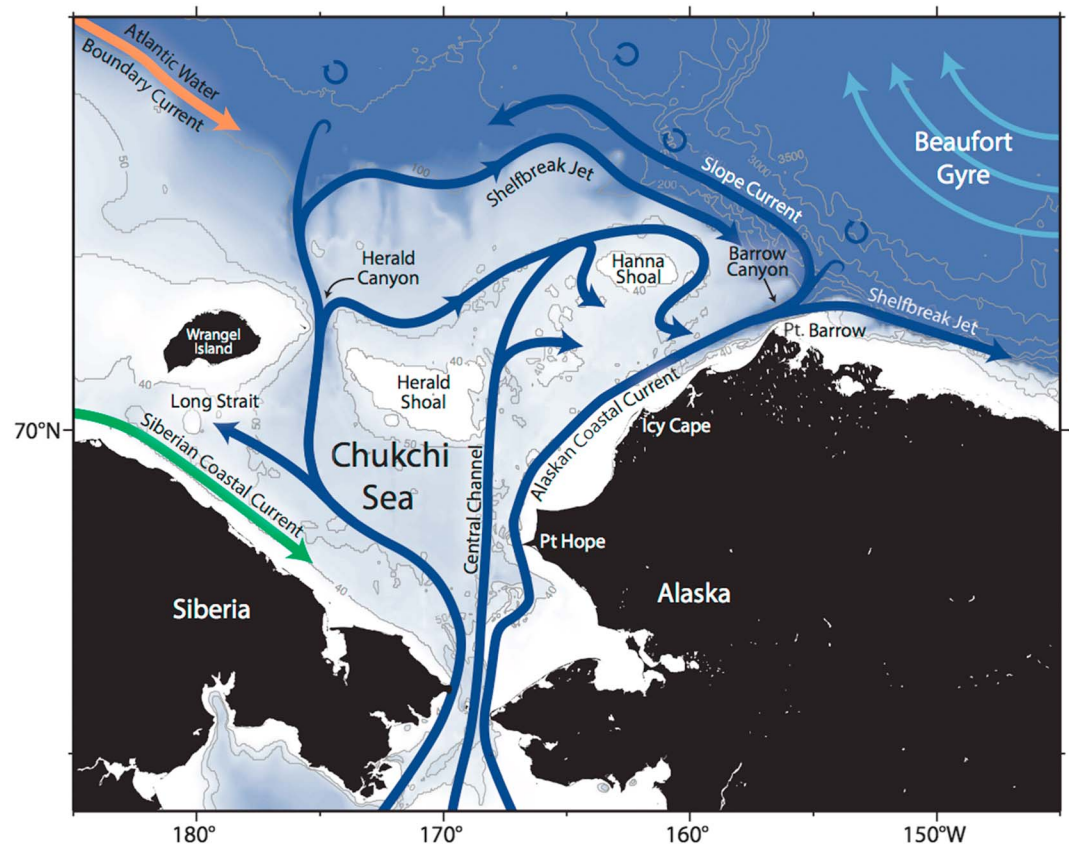


Figure 1. Map of the Pacific Arctic region showing major circulation, bathymetry, and location features referred to in the text.

2. Methods and Approach

2.1. Net Biological Production From $\Delta O_2/Ar$

The biological input/removal of O_2 during photosynthesis and respiration causes dissolved oxygen content of seawater to deviate from air-sea equilibrium. Dissolved oxygen saturation (ΔO_2), the ratio of observed oxygen concentration ($[O_2]_{meas}$) to oxygen concentration expected at solubility equilibrium ($[O_2]_{sat}$) set by temperature (T), salinity (S), and atmospheric pressure, allows these changes to be tracked easily:

$$\Delta O_2 (\%) = 100 \left(\frac{[O_2]_{meas}}{[O_2]_{sat}} \right) - 1. \quad (1)$$

However, in many oceanic settings biotic saturation changes are convoluted by abiotic factors which also influence ΔO_2 . For example, a recent warming or cooling of the surface ocean would cause O_2 to be temporarily supersaturated or undersaturated, respectively, as the new solubility equilibrium changes. Breaking waves and bubble injection also cause abiotic gas supersaturation (Hamme & Emerson, 2002; Stanley et al., 2009). These abiotic effects drive saturation change of similar magnitude to biotic effects in all but the most intensely productive systems.

Observations of O_2/Ar saturation ($\Delta O_2/Ar$) allow biotic forcing to be separated from the total gas saturation (ΔO_2) since the inert gas Ar tracks abiotic saturation changes (e.g., Craig & Hayward, 1987; Kaiser et al., 2005):

$$\Delta O_2/Ar (\%) = 100 \left[\left(\frac{O_2}{Ar} \right)_{meas} / \left(\frac{O_2}{Ar} \right)_{sat} - 1 \right], \quad (2)$$

where $\left(\frac{O_2}{Ar} \right)_{meas}$ is the measured ratio and $\left(\frac{O_2}{Ar} \right)_{sat}$ the solubility equilibrium ratio (Garcia & Gordon, 1992; Hamme & Emerson, 2004). The $\left(\frac{O_2}{Ar} \right)_{meas}$ can be determined at sea near-continuously using a quadrupole

mass spectrometer interfaced to a system for gas extraction from surface seawater (equilibrated inlet mass spectrometer, EIMS; Cassar et al., 2009). The quotient $\Delta O_2/Ar$ represents the net biologically driven O_2 saturation. A $\Delta O_2/Ar > 0$ indicates a net autotrophic community, with positive net community production (NCP) implied, and $\Delta O_2/Ar < 0$ indicates a heterotrophic community ($NCP < 0$). The residence time of dissolved O_2 in the surface mixed layer with respect to gas exchange (which drives ΔO_2 and $\Delta O_2/Ar$ toward equilibrium) is typically ~ 2 weeks, a function of the ratio of mixed layer depth to the gas transfer rate (k_{O_2}). Therefore, $\Delta O_2/Ar$ indicates the time-integrated net metabolism over this timeframe (Kaiser et al., 2005; Teeter et al., 2018).

We continuously monitored ΔO_2 and $\Delta O_2/Ar$ in surface seawater of the Pacific Arctic sector on two *USCGC Healy* cruises in October 2011 and 2012. Details of analysis are similar to previous studies (Cassar et al., 2009; Hamme et al., 2012) and are reported with online data (arcticdata.io, doi:10.18739/A21G22). Briefly, the $\Delta O_2/Ar$ was determined by EIMS measurement of seawater supplied from the surface underway system (nominal intake at 8 m) through several coarse filters to a small contactor membrane (Liquicel Micromodule G569) from which a $2\text{ m} \times 0.5\text{ }\mu\text{m}$ OD-fused silica capillary sampled equilibrated sample air in the contactor headspace. Ion current ratios were monitored with a Pfeiffer Prisma Plus QMA 220 and the O_2/Ar ion current ratio was calibrated with outside air measured every 2 hr. Measurements were binned into ca. 2-min intervals, for an effective sampling resolution of ~ 0.5 km during ship transits. Bottle samples were drawn twice daily from the underway seawater flow and stored for later analysis. Shore-side, $\Delta O_2/Ar$ was determined on bottle samples using a Thermo 253 Isotope Ratio Mass Spectrometer (as in Juranek et al., 2012). EIMS-based $\Delta O_2/Ar$ observations were evaluated against time-matched bottle samples for potential offsets. The majority of the data did not require any offset correction, with bottle samples matching EIMS- $\Delta O_2/Ar$ within uncertainty of bottle-based measurements ($\pm 0.3\%$) and no evidence of bias. However, after notable system events (e.g., restarting after power interruption, filament change, contactor membrane change) offsets between bottle and EIMS- $\Delta O_2/Ar$ were sometimes evident. To correct EIMS- $\Delta O_2/Ar$, all bottle data over the affected time period were averaged to determine a mean correction (as in Hamme et al., 2012). Standard error of these corrections, based on groupings of 4–8 bottle samples, was less than 0.2%. Details of these offset corrections are discussed in the documentation provided with data at arcticdata.io (doi:10.18739/A21G22).

To constrain ΔO_2 , we utilized a Seabird Scientific SBE43-dissolved oxygen sensor maintained as part of flow-through sensor suite by the *Healy* shipboard scientific technical support group. The sensor data were corrected using Winkler surface seawater samples collected from the surface underway periodically throughout the cruise. Details on these corrections are also available with the online data documentation.

2.2. Surface Seawater pCO_2 Observations

To evaluate the impact of net biological CO_2 uptake on Pacific Arctic air-sea CO_2 exchange we compare $\Delta O_2/Ar$ with the observed sea-air pCO_2 disequilibrium ($\Delta pCO_2 = pCO_{2\text{ sw}} - pCO_{2\text{ atm}}$, where subscripts refer to surface seawater and atmosphere, respectively). Surface $pCO_{2\text{ sw}}$ was measured near-continuously on 2011 and 2012 *Healy* cruises using a shower-type air-seawater equilibrator system similar to that described by Sutherland et al. (2017). The nondispersive infrared CO_2 analyzer was calibrated every 6 hr using five reference CO_2 -air mixtures (CO_2 concentrations ranging from 150 to 750 ppm) certified by the NOAA/Earth System Research Laboratory, Boulder, CO. All surface $pCO_{2\text{ sw}}$ data, as well as details on data processing, are available online (Takahashi et al., 2017, and www.ldeo.columbia.edu/CO2). Because measured $pCO_{2\text{ atm}}$ on 2011 and 2012 *Healy* cruises were often contaminated with ship exhaust, we computed ΔpCO_2 using monthly averaged $pCO_{2\text{ atm}}$ measured at the Barrow (United States) Meteorological Station (389 and 394 ppm mole fraction in dry air in October 2011 and 2012, respectively, NOAA ESRL Global Monitoring Division, 2016) corrected for the monthly mean barometric pressure from NCEP Reanalysis provided by NOAA ESRL (<http://www.esrl.noaa.gov/psd/>).

2.3. Meteorological Products

We obtained wind products (u and v components for wind referenced to 10 m above the sea surface) from the NCEP North American Regional Reanalysis provided by NOAA/OAR/ESRL Physical Sciences Division, Boulder, Colorado, United States, website at <http://www.esrl.noaa.gov/psd/>. Daily-averaged directional components were used to determine gridded wind speed for the timeframe corresponding to 2011 and

2012 observations as well as up to 60 days prior. Wind speed history was used to evaluate presence of storm events for our region of study, as well as to calculate gas exchange rates for O_2 and CO_2 (as described in section 6).

3. Regional Setting

The study area included three Pacific Arctic marginal seas—northern Bering, Chukchi, and western Beaufort (Figure 1)—with distinct identities in terms of water masses, circulation, and biogeochemical functioning (Carmack & Wassmann, 2006; Danielson et al., 2014; Grebmeier et al., 2015). We briefly recap a few features of the regional oceanography to orient discussion. Near the southernmost end of the survey, Bering Strait is a physically energetic narrow (~85 km), shallow (~50 m) channel with a long-term mean northward flow of ca. 0.8 Sv (Roach et al., 1995; Woodgate et al., 2015). Interannual variations in the northward transport at this Pacific Arctic gateway (e.g., 0.7 Sv in 2012 and 1.1 Sv in 2011) have important implications for nutrient, heat, and freshwater budgets downstream in the Chukchi and more generally in the Arctic basin (Woodgate et al., 2012). In summer, three water masses that influence the Chukchi and Beaufort seas flow through Bering Strait (Coachman et al., 1975). The warm, fresh ($S < 31$), and nutrient-poor Alaskan Coastal Water (ACW) hugs the Alaskan coast on the eastern side of Bering Strait (Figure 1) as a buoyancy current fed by the seasonal discharge of Alaskan rivers (Woodgate et al., 2012, 2015). On the opposite, western side of Bering Strait, the colder, nutrient-rich, and more saline ($S \sim 33$) Anadyr Water (Coachman et al., 1975) derived from the deep basin and Bering Slope Current waters that are mixed to the surface in the Gulf of Anadyr carries an important reservoir of nitrate (NO_3^-) into the Pacific Arctic (Grebmeier et al., 2015; Sambrotto et al., 1984; Walsh et al., 1997; Woodgate et al., 2015). Interannual variability in Anadyr Water is one large-scale “remote forcing” determinant of potential PP in this region (Danielson et al., 2017; Tremblay et al., 2015). In the mid-Strait, northward flowing waters that previously occupied the broad Bering Shelf flow north in summer. This water mass is slightly less saline than Anadyr water ($S \sim 32.5$) and typically depleted of the limiting nutrient NO_3^- in the upper ~20 m (e.g., above the pycnocline), by the ice-retreat bloom over the broad Bering Sea shelf (Grebmeier et al., 2015). Below the pycnocline, Bering Shelf water is typically slightly more saline (e.g., not influenced by freshwater inputs) and contains low O_2 , high pCO_2 , and high nutrient concentrations accumulated from remineralization of sinking particles on the Bering Shelf (Grebmeier et al., 2015).

The energetic flow through the Bering Strait choke point induces enhanced mixing in this region (Grebmeier et al., 2015; Woodgate et al., 2015). Flow interaction with bathymetry and promontories north of Bering Strait in the southern Chukchi can induce lateral and vertical mixing of the aforementioned water masses. While ACW mostly retains its distinct identity in the northward flowing Alaska Coastal Current, Anadyr Water and Bering Shelf Water are generally collectively referred to as Bering Summer Water (BSW) north of Bering Strait. In addition, surface flow responds rapidly to local wind forcing, resulting in occasional off-shore Ekman transport of ACW as well as wholesale changes in current direction for a week or more (Aagaard et al., 1985; Danielson et al., 2014; Pisareva et al., 2015; Woodgate et al., 2015). These processes help to maintain high spatial variability in distributions of T , S , nutrients, and other biogeochemical parameters in the southern Chukchi.

Downstream of Bering Strait, water mass properties are subsequently modified to varying degrees by warming/cooling, sea ice melt, mixing, and biological uptake/removal during months of transit over the broad, shallow (~50 m) Chukchi shelf (Pickart et al., 2016; Shroyer & Pickart, 2018). The extent and timing of sea ice melt in particular plays a significant role in water column stratification, which in turn impacts potential for surface phytoplankton communities to access inorganic nutrient reservoirs beneath the halocline/pycnocline after surface reservoirs are exhausted (e.g., Danielson et al., 2017; Lowry et al., 2015; Weingartner et al., 2017). For example, an anomalously early sea ice retreat in 2011 led to a significantly reduced meltwater (MW) presence throughout the Chukchi shelf, while in 2012 a lingering ice presence resulted in substantial MW-influenced layer of 20 m capping the majority of the NE Chukchi, with stratification nearly twice as strong in 2012 versus 2011 (Weingartner et al., 2017). Wind strength, direction, and persistence also play a significant role in residence time and physical modification of water masses in this region (Danielson et al., 2017). Persistent northerly or easterly winds can cause the typical circulation (Figure 1) to stall or reverse. Strong easterly winds can promote shelfbreak upwelling along the narrow

Beaufort shelf; during these episodes the NE Chukchi often experiences intrusions of more saline, nutrient-rich Atlantic-origin water ($S > 33.6$) from the halocline of the Beaufort Sea via the conduit of Barrow Canyon (e.g., Pickart et al., 2013). Because the above processes can cause conditions at a given location to differ significantly from year to year (and over daily time scales), data collected over multiple years are best interpreted within the context of the mean circulation (Figure 1) as well as differences in water mass presence at the time of observation.

4. Spatial and Temporal Trends in Net Biological Production From $\Delta O_2/Ar$

4.1. Spatial Patterns

Within this physical framework, observations of $\Delta O_2/Ar$ in 2011 and 2012 give an unprecedented view of spatial patterns and potential drivers of net biological production in the late season Pacific Arctic (Figures 2–5). Regionally, the northern Bering and southern Chukchi were characterized by mesoscale variability in $\Delta O_2/Ar$ and significant deviations in $\Delta O_2/Ar$ values from equilibrium, as expected given the circulatory framework described above (Figures 2 and 4). Large negative $\Delta O_2/Ar$ extrema were associated with higher salinity, higher pCO_2 , and (where measured) nutrient concentrations, indicating likely vertical mixing of O_2 -poor and CO_2 - and nutrient-rich bottom-layer water to the surface. Positive extrema were also concentrated in the Bering Strait and southern Chukchi, particularly in the vicinity of Pt Hope (Figures 1, 3, and 5), a previously identified biological hotspot believed to be fueled by lateral/vertical intrusions of nutrients and a reduced current velocity and turbulence regime north of Bering Strait (Grebmeier et al., 2015). The high spatial resolution afforded by the continuous underway $\Delta O_2/Ar$ mapping provides insight into potential fronts and mixing hotspots that would otherwise be missed by coarser resolution approaches in this highly variable region.

In contrast, observations of $\Delta O_2/Ar$ in the northern Chukchi and western Beaufort Seas had less extreme deviations from equilibrium (Figures 2–5). In each year, early October observations were predominantly weakly autotrophic ($\Delta O_2/Ar$ of $\sim 1 \pm 0.5\%$), with an increasing proportion of $\Delta O_2/Ar$ indicating net heterotrophy in late October during the return transit. The low $\Delta O_2/Ar$ values are comparable to those typically found in low nutrient, low chlorophyll oligotrophic regions where microbial recycling dominates (Juranek & Quay, 2005; Quay et al., 2010) and consistent with a nutrient-limited phytoplankton community expected in this region in late season (Grebmeier et al., 2015; Tremblay et al., 2015). Indeed, concentrations of dissolved NO_3^- were below detection throughout much of the NE Chukchi (Figures 3 and 5), while measurable quantities of nonlimiting nutrients phosphate and silicate remained (data not shown).

However, patches of moderate $\Delta O_2/Ar$ (e.g., $+2$ – 4%) were observed in the NE Chukchi, including the vicinity of Hanna Shoal and Barrow Canyon (Figures 3 and 5). Both of these locales are within the boundary of the NE Chukchi Sea benthic biological hotspot identified by Grebmeier et al. (2015). The factors contributing to increased benthic biomass at Hanna Shoal have not been clearly identified (suggested mechanisms include topographic steering and flow-bathymetry interactions over this shallow feature). In contrast, the linkages between biological productivity at the Barrow Canyon hotspot are more well-known (Ashjian et al., 2010; Hill & Cota, 2005; Pickart et al., 2013). Frequent episodes of strong easterly winds drive shelf-break upwelling of nutrient-rich Atlantic-origin water ($S > 33.6$) from beneath the halocline of the Beaufort basin onto the shelf and up Barrow Canyon into the NE Chukchi. The influence of Atlantic Water during these events can extend well into the Chukchi, as far south as Icy Cape (Figure 1; Ladd et al., 2016).

4.2. Temporal Patterns and Relationship to Meteorological Forcing

Temporal changes between northbound and southbound transits allow some assessment of the immediate impacts of passing storm systems on surface $\Delta O_2/Ar$ values. North American Regional Reanalysis wind data indicate several passing storms influencing Pacific Arctic subregions each October (Figure 6 and animated Figures S1 and S2). In 2011, a strong storm with wind speeds exceeding 15 m/s occupied the NE Chukchi and W. Beaufort Seas for 8 days in mid-October (12–20 October); this event occurred after northbound sampling while *Healy* was in the eastern Beaufort conducting surveys under multiyear sea ice ($\Delta O_2/Ar$ data collected at this time were of poor quality and are not shown here), and just prior to the southbound transit. As previously documented, this storm induced significant upwelling of high $pCO_{2\text{ sw}}$ from the Beaufort basin

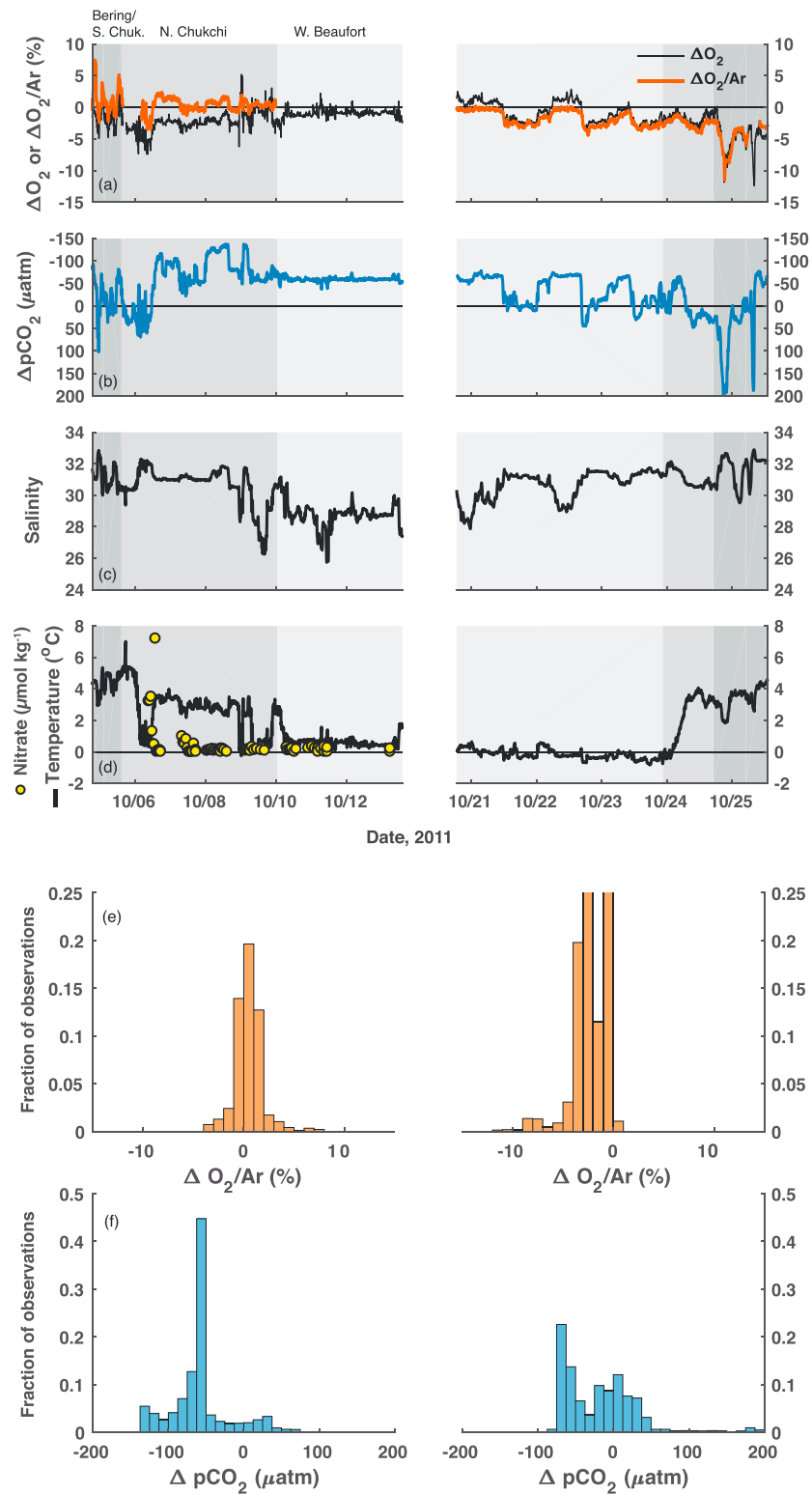


Figure 2. Observations collected during the 2011 *Healy* cruise: surface underway observations of (a) ΔO_2 and $\Delta O_2/Ar$, (b) ΔpCO_2 , (c) salinity, and (d) temperature. Nitrate concentration from surface bottle samples collected at conductivity-temperature-depth stations is also shown in panel (d). Background color shading indicates regions referred to in the text: northern Bering and southern Chukchi (64–69°N, darkest gray), northern Chukchi (>69°N and >156°W, medium gray), and western Beaufort (145–156°W, lightest gray). Panels (e) and (f) indicate data distribution histograms for $\Delta O_2/Ar$ and ΔpCO_2 , respectively, for northbound (left) and southbound (right) surveys.

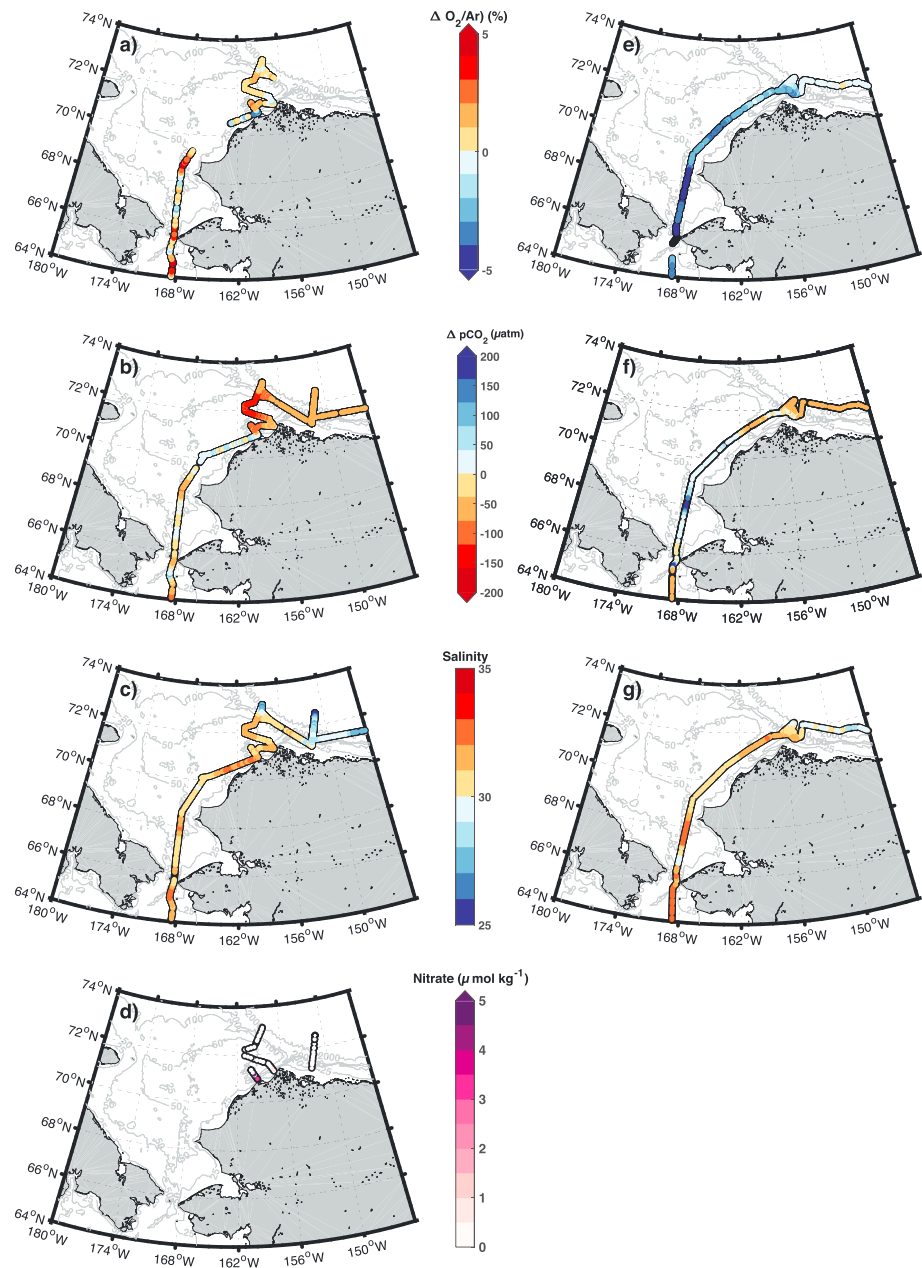


Figure 3. Maps of shipboard observations in 2011, allowing assessment of trends relative to circulation and bathymetry features: (a–d) $\Delta O_2/Ar$, ΔpCO_2 , salinity, and nitrate observed in early October during northbound transit, (e–g) same parameters (less nitrate) observed in late October during southbound transit. Note that the $\Delta O_2/Ar$ color scale has been truncated to a reduced range (–5% to +5%) to enable easier visualization of the more typical variations in $\Delta O_2/Ar$ as opposed to a handful of extreme values. The full range in $\Delta O_2/Ar$ is depicted in Figure 2. Nitrate color scale has also been truncated to enable detection of low, but nonzero concentrations.

halocline onto the continental shelf, resulting in an estimated outgassing of 0.2–0.5 TgC (Mathis et al., 2012). A separate event influenced the SW Chukchi 23–25 October, just prior to southbound sampling (Figure 6). The observed shift from predominantly positive to negative $\Delta O_2/Ar$ in all regions between northbound and southbound transits in 2011 (Figure 2) is consistent with the expected immediate impact of these storms. Enhanced turbidity, deeper mixed layers, and decreased light would tend to reduce photosynthesis, while remineralization of resuspended material and mixing of O_2 -depleted bottom water with the surface layer would all move $\Delta O_2/Ar$ toward less positive values. Similarly, in 2012, a strong storm event with wind

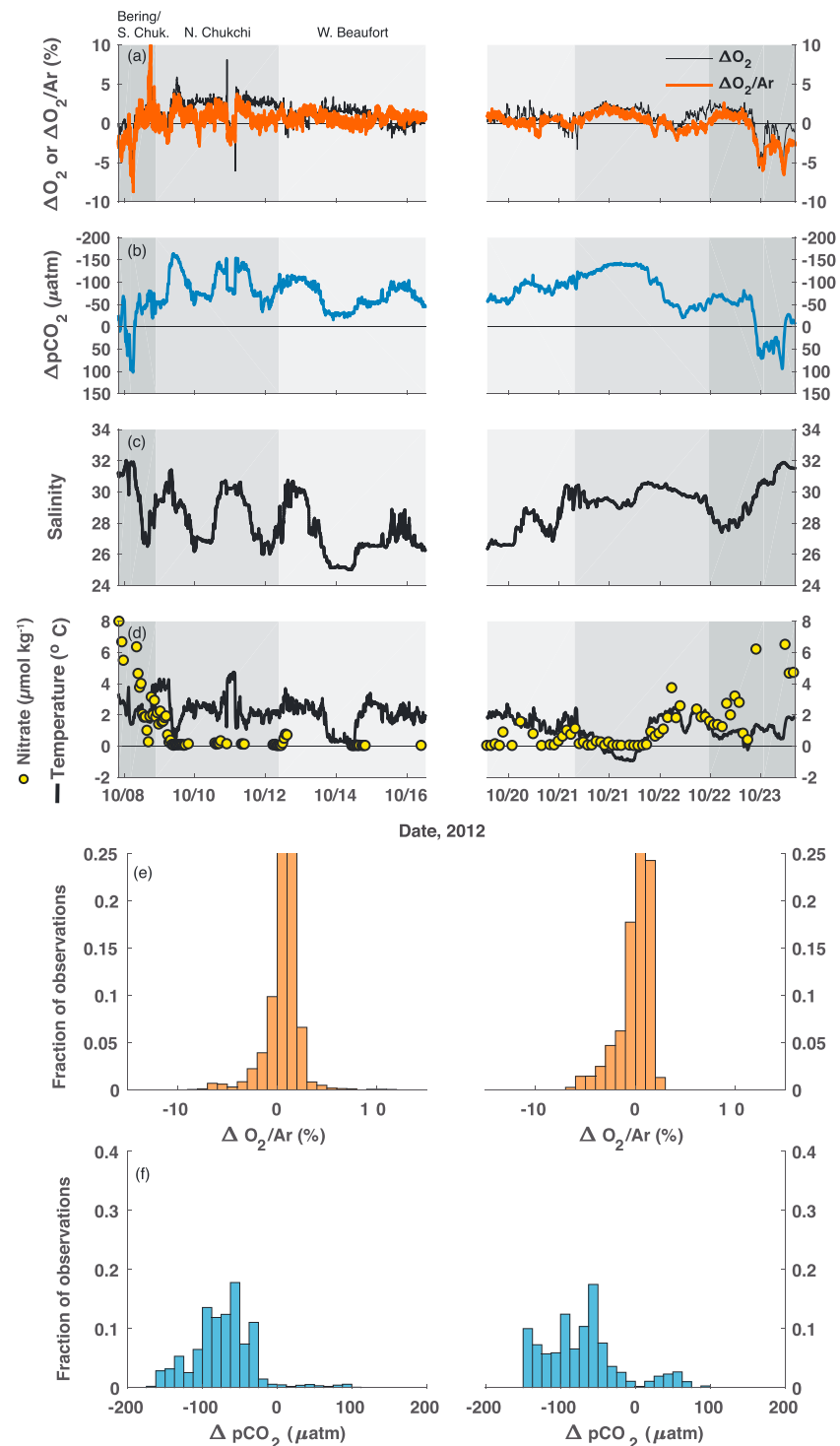


Figure 4. Same as in Figure 2, but for 2012 observations. Nitrate concentration shown in panel (d) were collected from the surface underway rather than CTD bottles.

speeds exceeding 15 m/s lingered over the Chukchi Sea for several days in late October (21–23), immediately prior to southbound sampling of this region (Figures 6 and S2). This storm might have contributed to the observed shift in $\Delta O_2/Ar$ conditions (Figure 4) between northbound and southbound transits, although observed changes were not nearly as large as in 2011.

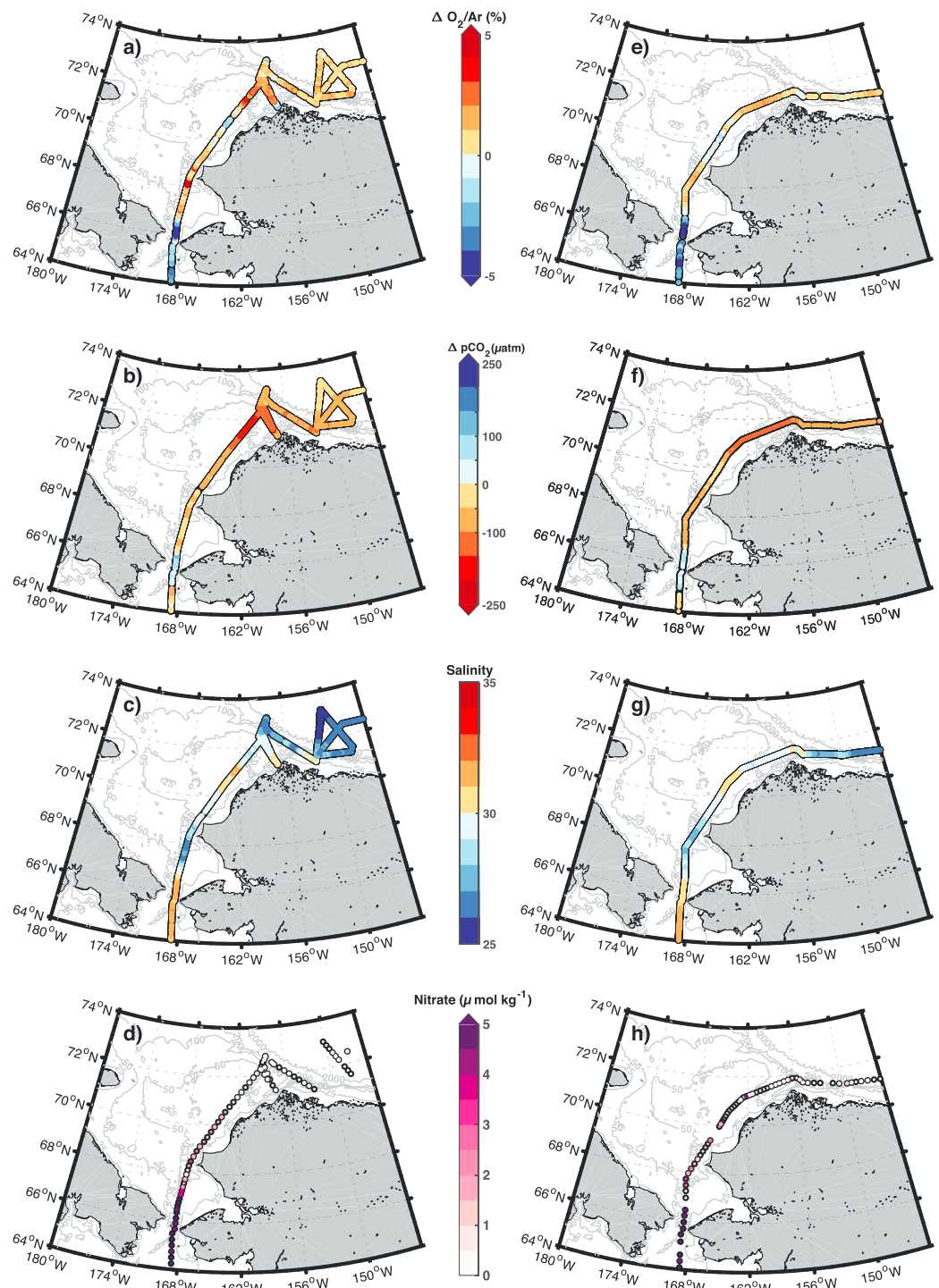


Figure 5. Same as in Figure 3, but for 2012 observations. Nitrate samples were collected during (d) northbound and (h) southbound transits in 2012.

In the context of our discussion regarding the importance of late season storms for supporting biological production over an extended growing season, it is important to be mindful of both the immediate impacts on biogeochemical distributions as well as the longer-term impact of these events. While a strong storm event can result in a momentary decrease in $\Delta O_2/Ar$ due to increased turbidity, decreased light, and mixing with unventilated O_2 -poor waters from beneath the pycnocline, the response of the surface phytoplankton

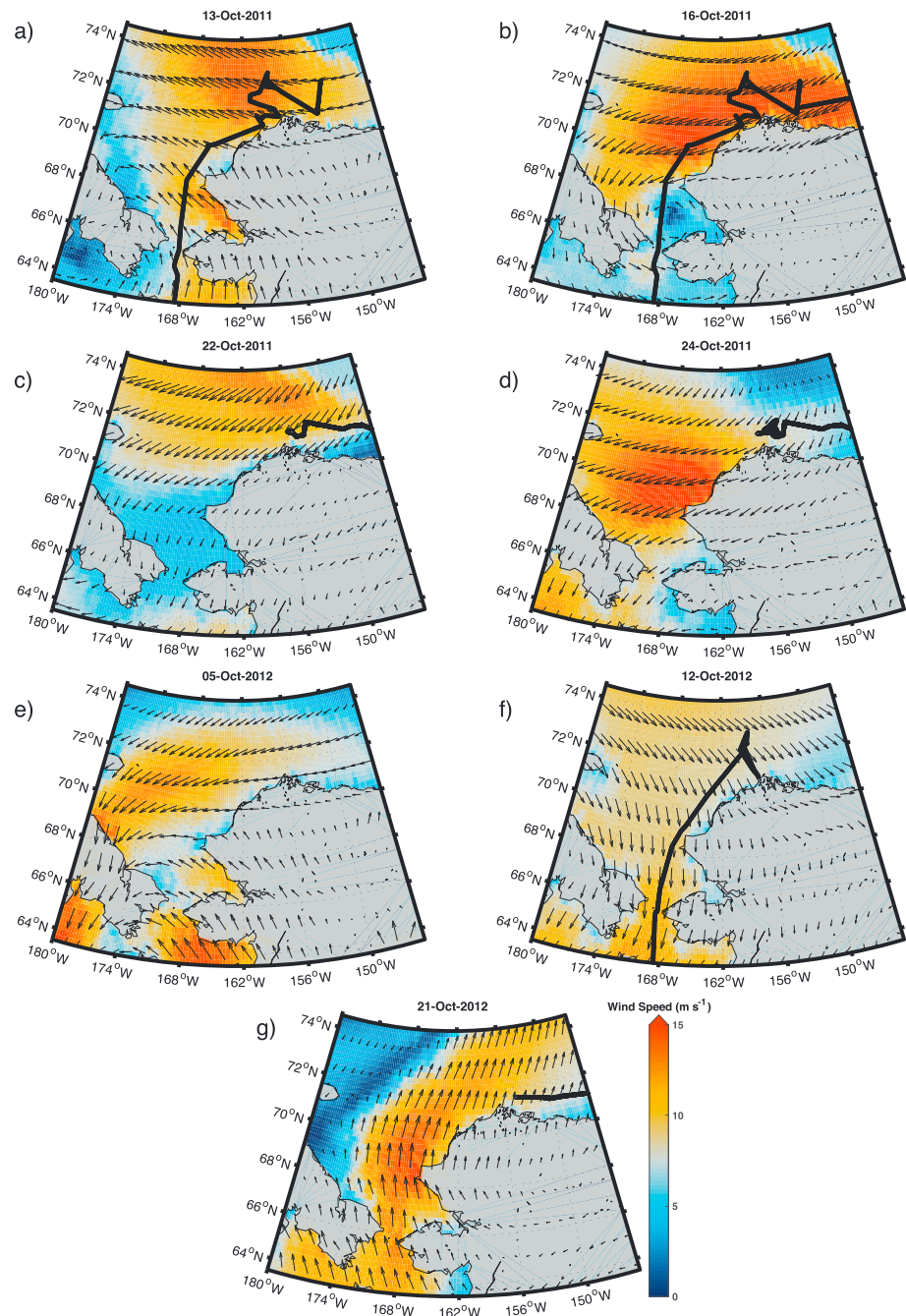


Figure 6. Selected maps of wind speed and direction in 2011 and 2012. Panels (a)–(c) show development, peak, and end of a large storm that influenced the region in mid-October 2011, between northern and southern transits. A second, separate event that affected the southern Chukchi just prior to southbound sampling is shown in panel (d). Panels (e)–(f) show wind speeds >10 m/s influencing the Chukchi prior to and during sampling in 2012. Panel (g) shows a storm in the southern Chukchi that occurred just prior to southbound sampling through this region. For complete movies of daily wind speed and direction relative to ship position in October 2011 and 2012, please see supporting information.

community post-storm would presumably increase $\Delta O_2/Ar$ as light-quality improves and nutrients supplied by storm activity allow more growth. Even with the high degree of spatial resolution for $\Delta O_2/Ar$, attribution of longer-term biological response to any single storm event is difficult with only one or two snapshot realizations in time for a given locale, and observations that integrate the impact of frequent passing storm events of varying spatial domain and strength (Figures 6, S1, and S2). However, at a “big picture”

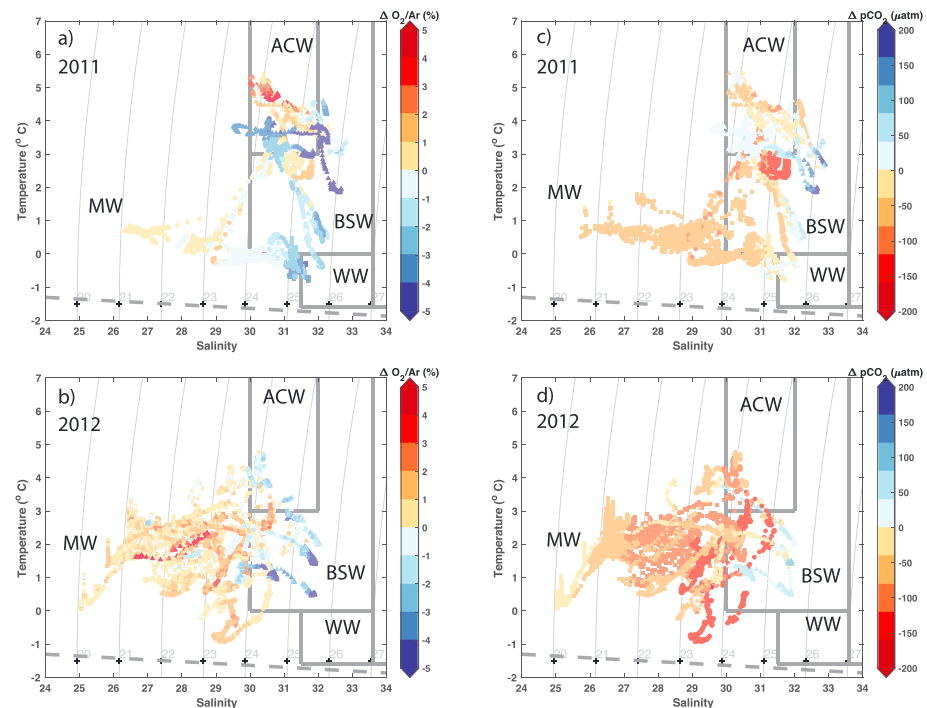


Figure 7. (a–b) Temperature-salinity relationships for surface data in 2011 and 2012, with color indicating $\Delta O_2/Ar$ (color scale truncated as in Figures 3 and 5), gray curved lines denote density; (c–d) temperature-salinity relationships colored by ΔpCO_2 . In all panels data from the northern Bering/southern Chukchi, N. Chukchi, and W. Beaufort are represented by triangles, circles, and squares, respectively. Water masses as defined by Pickart et al. (2019) are indicated by boxes with thick gray lines: MW = meltwater, ACW = Alaska Coastal Water, BSW = Bering Summer Water, WW = remnant winter water. WW is formed during the winter by convective mixing over the shelf and is subsequently warmed by mixing and heating throughout the summer (Pickart et al., 2019). WW is typically associated with bottom waters beneath the pycnocline in the NE Chukchi during summer.

level, observed biological hotspots of growth ($\Delta O_2/Ar > 2\%$) in a region that is perennially depleted in the limiting nutrient NO_3^- in late summer must be supported by a mechanism of nutrient supply. Figure 4 indicates higher surface $[NO_3^-]$ in the western Beaufort and northern Chukchi following storms in 2012 (12 and 21–21 October, Figures 6 and S2), lending some support to this proposed mechanism. The persistent storm activity in the late season Pacific Arctic and the body of literature associating these storms with enhanced turbulent mixing and/or nutrient supply (Nishino et al., 2015; Pickart et al., 2013; Rainville et al., 2011; Rainville & Woodgate, 2009) suggest that storm-induced delivery of nutrients should not be discounted.

4.3. Water Mass Patterns

Assessing 2011 and 2012 surface observations in T - S and O_2 space (Figure 7) allows some additional insight. Here we adopt water mass classifications following Pickart et al. (2019) to aid our interpretations. First, the reduced presence of sea ice melt-influenced water (MW) in 2011 compared to 2012, as noted by Weingartner et al. (2017) and described above, is apparent. More intriguingly, MW observations in 2012 tended to be more strongly autotrophic ($\Delta O_2/Ar > 0$), while heterotrophic ($\Delta O_2/Ar < 0$) observations were more commonly found in water masses with ACW and BSW characteristics (Figure 7). In 2011, heterotrophic activity was again associated with BSW, while a mixture of strongly autotrophic and strongly heterotrophic conditions were associated with ACW characteristics. However, these strongly autotrophic observations within the ACW were from two notable locations: (1) a region of high variability (and presumably mixing across water masses) in the northern Bering and southern Chukchi and (2) in the NE Chukchi near the head of Barrow Canyon off of Wainwright, AK (Figures 2 and 3). Both locations are subject to ephemeral intrusions of nutrients by processes described previously.

We also note that the most strongly heterotrophic observations in both years tended to be associated with the highest salinities observed in surface waters. This is consistent with our previously stated interpretation of these features being derived from mixing of unventilated, subsurface waters not previously influenced by sea ice melt at the surface.

While the relationships of $\Delta O_2/Ar$ and water masses to some extent confirm aspects of the large-scale regional circulation mentioned previously, association of autotrophic conditions with MW is unexpected. MW is typically regarded to be low in productivity and nutrient-deplete, and presence of MW enhances vertical stratification, reducing the prospect for diffusive mixing of nutrients from nutrient-replete subsurface waters into the surface. However, in September 2012, Weingartner et al. (2017) found variance in surface density fields increased twofold to fivefold in high-resolution transects in the MW-influenced region in the northern Chukchi compared to transects just south of the MW front. The authors attributed the enhanced density variance to (1) lateral processes involving MW that generate eddies and cross-frontal exchange in the pycnocline (Lu et al., 2015) and (2) spatial heterogeneity in sea ice floes, with corresponding variability in ice drag, melt rates buoyancy plumes. We further explore the relationship of our $\Delta O_2/Ar$ trends to variance in physical fields in section 7.

5. Relationships Between Net Biological Production and ΔpCO_2

5.1. Covariation of $\Delta O_2/Ar$ and ΔpCO_2

Patterns of oceanic CO_2 sink intensity (negative ΔpCO_2) and areas of high net biological O_2 production (positive $\Delta O_2/Ar$) exhibited remarkable spatial coherence in both years (Figures 2–5). The covariance is especially evident in point-by-point comparisons (Figure 8), where a model II linear regression indicates significant correlation in both years (correlation coefficient $r = -0.74$ and -0.61 for 2011 and 2012, respectively). Given the coupling between CO_2 and O_2 in photosynthesis/respiration, this may not be surprising; however, the very different time scales of O_2 and CO_2 with respect to air-sea gas exchange make this result more compelling. The longer residence time of CO_2 in the upper ocean, a result of $pCO_{2,sw}$ equilibration with the large total dissolved inorganic carbon (DIC) reservoir, causes surface $pCO_{2,sw}$ to be affected by abiotic (warming/cooling) and biotic forcing (photosynthesis/respiration) over several months (Takahashi et al., 2002, 2009). Thus, the correlation of $\Delta O_2/Ar$ signal of more recent origin with ΔpCO_2 accumulated over a seasonal time scale suggests a significant impact of late season biological carbon uptake on the air-sea CO_2 gradient.

We graphically explore the potential contributions from biotic and abiotic drivers of ΔpCO_2 in more detail in Figure 9. Consider a hypothetical scenario where the area sampled was in equilibrium with the atmosphere prior to our sampling ($\Delta O_2/Ar = 0$, $\Delta pCO_2 = 0$): abiotic mechanisms such as warming/cooling would cause ΔpCO_2 to increase/decrease independently of $\Delta O_2/Ar$, as indicated (Figure 9, for details of calculations see figure legend). In contrast, biological production/removal of O_2 would cause $\Delta O_2/Ar$ and ΔpCO_2 to increase/decrease in an anticorrelated fashion, although with shallower slope than indicated by observations. If we instead assume a nonzero origin for ΔpCO_2 from biological activity that predates the time-integration of $\Delta O_2/Ar$ (e.g., the y-intercept of the 2012 model II regression) and allow biological additions/removals corresponding to $\Delta O_2/Ar$ as before, a similar, but offset trend results. Therefore, to achieve a slope similar to that observed in 2011 and 2012, some combination of biotic and abiotic modification is required. This could be achieved in a variety of ways, such as warming of recently upwelled water masses with high ΔpCO_2 and negative $\Delta O_2/Ar$ and cooling of surface waters with high $\Delta O_2/Ar$ and negative ΔpCO_2 . Differences in seasonally integrated forcing on ΔpCO_2 between regions can also introduce variability in the “origin” from which more recent coupled trends in ΔpCO_2 and $\Delta O_2/Ar$ evolve. A breakdown of trends for each region indicates some differences in the clustering of data in ΔpCO_2 and $\Delta O_2/Ar$ space (although regional relationships broadly follow the Pacific Arctic sector trend, Figure S3). Equilibration with the atmosphere by air-sea gas exchange would act to steepen the observed slope, because $\Delta O_2/Ar$ would be forced toward zero much more rapidly than ΔpCO_2 because of its faster equilibration time scale.

5.2. Use of ΔAr to Explore Abiotic Effects on ΔpCO_2 and $\Delta O_2/Ar$ Relationship

Some insight into potential contributions from recent warming and cooling is achieved by combining $\Delta O_2/Ar$ with total gas saturation (ΔO_2) to derive ΔAr , which isolates the gas saturation driven by abiotic processes

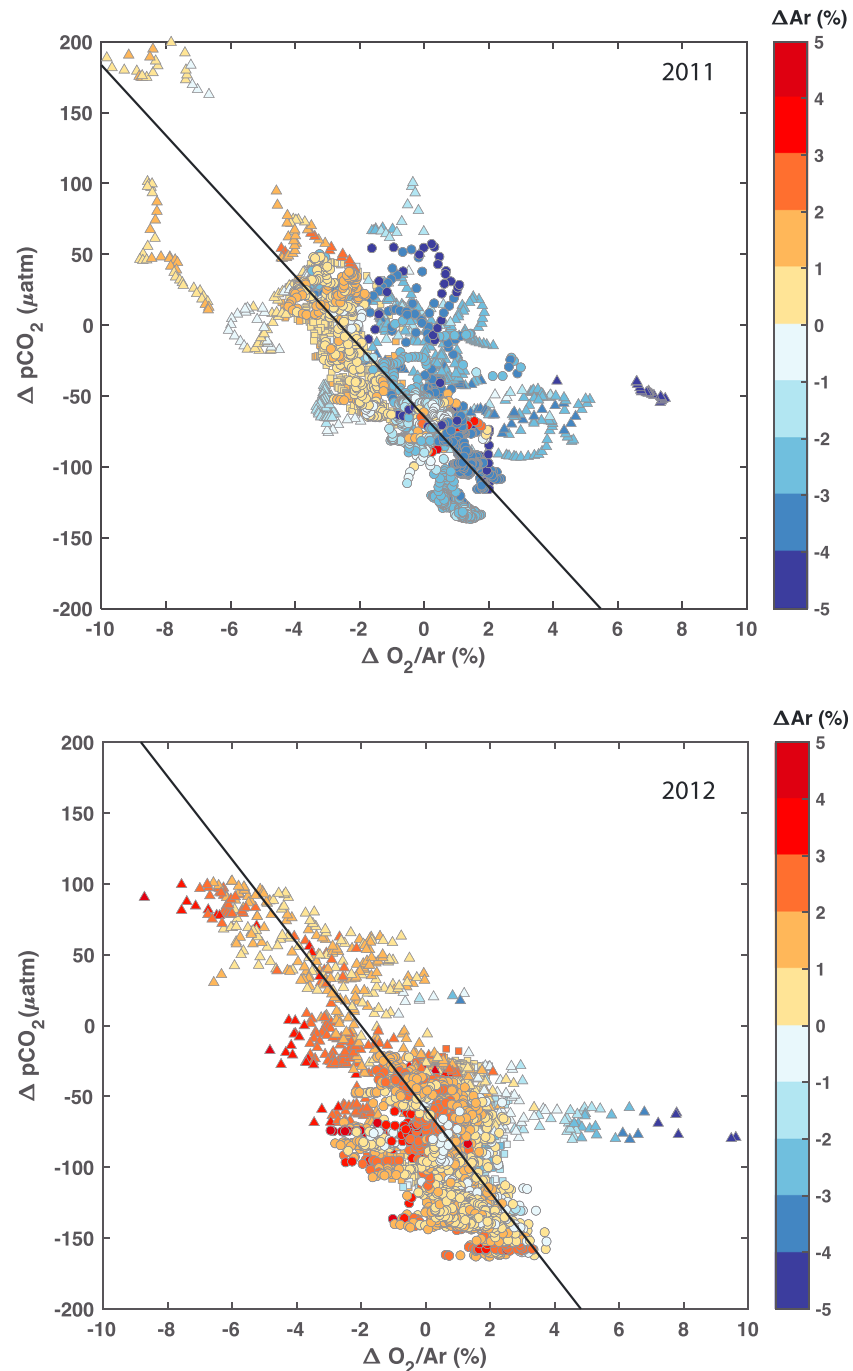


Figure 8. Relationship between $\Delta O_2/Ar$ and ΔpCO_2 in surface observations from 2011 and 2012. Thick black line shows the model II geometric mean regression in each year. Observations are colored by physical gas saturation (ΔAr), computed from $\Delta O_2/Ar$ and ΔO_2 , as discussed in text. Triangles, circles, and squares indicate data collected in the N. Bering/S. Chukchi, N. Chukchi, and W. Beaufort, respectively.

(Eveleth et al., 2014, 2017). Mapping ΔAr onto our $\Delta O_2/Ar$ and ΔpCO_2 trends (Figure 8) allows some intriguing relationships to emerge. First, the highest $\Delta O_2/Ar$ values in both years were associated with most negative physical saturation (ΔAr approaching -5%). Second, high $pCO_{2\ sw}$ (positive ΔpCO_2) and biological undersaturation ($\Delta O_2/Ar < 0$) were associated with physical supersaturation (positive ΔAr). Finally, a clear temporal shift to a more positive ΔAr at the end of October is evident for both years (Figure S4).

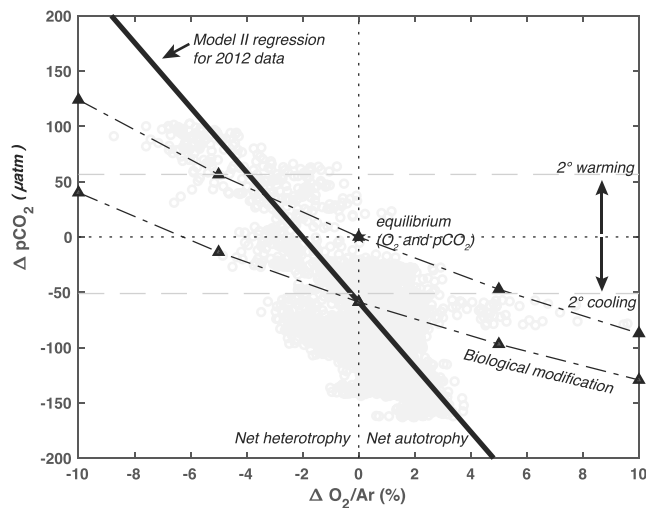


Figure 9. Schematic exploring processes impacting $\Delta O_2/Ar$ and ΔpCO_2 , including warming (affects ΔpCO_2 only) and biological additions/removals from two different origins (affects $\Delta O_2/Ar$ and ΔpCO_2). Light gray data points are surface $\Delta O_2/Ar$ and ΔpCO_2 observations from 2012. Calculations assume $T = 2^\circ C$, $S = 32$, and $[O_2]_{sat} = 340 \mu mol/kg$. To determine biological impact on pCO_2 we first determined DIC for a system in equilibrium with the atmosphere ($pCO_2_{sw} = 394 \mu atm$) using a total alkalinity of $2110 \mu mol/kg$ (e.g., comparable to surface values observed in the NE Chukchi in 2012, Mathis et al., 2015). We then calculated addition/removal of DIC corresponding to given O_2 changes using a $-\Delta O_2/\Delta CO_2 = 1.2$ (Laws, 1991; we chose this value to account for growth supported by both NO_3^- and NH_4^+ given significant concentrations of both in bottom waters). We then calculated new pCO_2_{sw} from DIC and TA assuming negligible impact of biological activity on total alkalinity. These calculations were repeated assuming a second case with an initial ΔpCO_2 disequilibrium equivalent to the y-intercept of the model II regression for 2012 ($\Delta pCO_2 = -64 \mu atm$, $pCO_2_{sw} = 330 \mu atm$).

A number of processes can cause a physical gas undersaturation, including recent cooling, freshening, sea ice melt, and increasing atmospheric pressure (e.g., Eveleth et al., 2014; Hamme & Emerson, 2004). For example, a recent T decrease from 4 to $2^\circ C$ would drive a 5% physical undersaturation in Ar (and O_2). Sea ice melt is depleted in O_2 and Ar since both are excluded from the sea ice matrix during freezing; taking a pure sea ice melt endmember ΔAr of -45% (Top et al., 1985, 1988), a ΔAr of -5% could be achieved by a 10% fractional contribution of melt in the surface layer (i.e., 2 m melt in a typical 20 m mixed layer). However, sea ice melt is an unlikely culprit for ΔAr undersaturations observed in 2011 because sea ice retreat occurred very early (i.e., mid-June, Weingartner et al., 2017) and any disequilibrium imparted by melt would be equilibrated with the atmosphere in the intervening time. In 2012, ice lingered over the NE Chukchi into mid-September, but the most undersaturated ΔAr values were observed in the southern Chukchi, a region clear of ice by July. Alternatively, a recent increase in sea level pressure of ~ 50 mbar or a S decrease of 7 could also result in a ΔAr of -5% . Likely, some combination of the above factors contribute to observed ΔAr , but a recent $2^\circ C$ cooling for much of this region is consistent with T differences between our study and observations reported for mid-September 2011 and 2012 (Danielson et al., 2017; Weingartner et al., 2017) as well as NOAA AVHRR Blended Daily high-resolution sea surface temperature throughout September/October (Reynolds et al., 2007; see animated Figures S5 and S6).

The association of high pCO_2_{sw} (positive ΔpCO_2) and negative $\Delta O_2/Ar$ with physical supersaturation ($\Delta Ar > 0$), particularly in the latter half of October (Figure S4) also warrants discussion. Physical supersaturations are caused by the opposite of the undersaturation mechanisms described above (warming, increasing S , sea ice formation, and decreasing atmospheric pressure) as well as two other processes: bubble collapse/exchange from breaking waves and mixing of water masses with

different gas solubility equilibria (Emerson et al., 2012; Eveleth et al., 2014; Hamme & Emerson, 2004). The mixing effect is a consequence of the concave shape of the O_2 and Ar solubility curve, which results in a supersaturation for conservative mixing behavior. As discussed previously, the majority of positive ΔpCO_2 (and accompanying negative $\Delta O_2/Ar$) occurred as mesoscale excursions coincident with higher S and lower T , which we take to be indicative of localized mixing with unventilated waters carrying a low O_2 and high pCO_2_{sw} signal from accumulated remineralization of organic matter. Therefore, ΔAr supersaturations may be due in part to mixing of surface and subsurface waters with different solubility endmembers. Another likely factor is that the ΔAr signal in subsurface water will reflect conditions that occurred when the water mass was last in contact with the atmosphere. During sea ice formation ΔAr increases due to exclusion of gases from the sea ice matrix (Top et al., 1985, 1988), while exclusion of CO_2 and precipitation of the $CaCO_3$ mineral ikaite would also increase pCO_2_{sw} (Rysgaard et al., 2011). An increase in pCO_2_{sw} without a corresponding change in $\Delta O_2/Ar$ would act to steepen the relationship between these two variables, which together with recent cooling for surface (low pCO_2_{sw} and higher $\Delta O_2/Ar$ samples) may in part explain the observed slope in 2011 and 2012.

While it is difficult to decompose the relationship between $\Delta O_2/Ar$ and ΔpCO_2 into exact contributions from biotic and abiotic factors, the potential impact of recent biological activity on ΔpCO_2 is clear. For every 1% increase in $\Delta O_2/Ar$, ΔpCO_2 is calculated to decrease by $\sim 10 \mu atm$ (Figure 9). For biological hotspots where $\Delta O_2/Ar$ approached 10% and ΔpCO_2 approached $70 \mu atm$ in both years, 100% of the air-sea CO_2 gradient could be explained by recent productivity recorded by $\Delta O_2/Ar$. More generally, for all observations where CO_2 uptake was indicated ($\Delta pCO_2 < 0$) in 2011 and 2012 surveys, $>40\%$ of sites in 2011 and $>50\%$ in 2012 were associated with a significant contribution from recent biological productivity (e.g., at least 10% of ΔpCO_2 explained by concurrent $\Delta O_2/Ar$).

6. Air-Sea CO₂ Flux and Estimated NCP

6.1. NCP Rates and Comparison to Prior Estimates

High-resolution $\Delta O_2/Ar$ data reported here also offer a unique opportunity to estimate NCP rates along the 2011 and 2012 surveys since net input or loss of O₂ via photosynthesis and respiration is stoichiometrically related to net production of organic carbon, that is, $CO_2 + H_2O \rightarrow CH_2O + O_2$. To derive NCP rates, $\Delta O_2/Ar$ data are interpreted within the context of surface mixed layer oxygen mass balance, and a biological production-gas exchange steady-state is assumed (Kaiser et al., 2005):

$$NCP \text{ (mmol O}_2 \text{ m}^{-2} \text{ d}^{-1}) = k_{O_2} O_{2 \text{ sat}} [\Delta O_2/Ar]/100, \quad (3)$$

where k_{O_2} is the gas transfer coefficient (m/day) for O₂ determined from wind speed (Wanninkhof, 2014). Note that the above expression assumes all $\Delta O_2/Ar$ signals are generated in the surface and does not explicitly account for vertical mixing, which can bias surface $\Delta O_2/Ar$ (typically toward more negative values, as subsurface waters in this region tend to be O₂-poor). We refrain from estimating NCP for data that appear to have a strong vertical mixing bias, defined here as satisfying both criteria: $\Delta O_2/Ar < -2\%$ and $\Delta pCO_2 > 0$. The derivation of equation (3) from O₂ mass balance also includes an assumption that $\Delta Ar = 0$ (see Eveleth et al., 2014; Kaiser et al., 2005, for details); this introduces a small, proportional error into our calculations when ΔAr deviates from 0 (<5% for ΔAr observed here). Because of the relatively simple physical framework used to convert observations of $\Delta O_2/Ar$ into NCP rates, estimates reported here should be approached with some caution. However, $\Delta O_2/Ar$ -based NCP do provide meaningful order of magnitude estimates for biological CO₂ sequestration during the data-poor late open water period and are useful in comparisons with prior earlier season estimates. For more details on NCP calculation, including an expanded discussion of uncertainties, we refer the reader to the online supplement.

Distributions of NCP were similar to trends in $\Delta O_2/Ar$ discussed in section 4. The >9,000 NCP rates calculated for the study area occupied a broad range (−60 to 100 mmol O₂·m^{−2}·day^{−1}, Figure 10), with the highest NCP rates associated with previously described $\Delta O_2/Ar$ “hotspots” in the northern Bering and southern Chukchi (northbound transits in 2011, 2012). In the northern Chukchi, NCP rates were lower, but a sizeable fraction of observations occupied a moderate NCP range of 10–20 mmol O₂·m^{−2}·day^{−1}. The observed rates in these hotspots are broadly consistent with those inferred by Pickart et al. (2013) from NO₃[−] supply associated with upwelling events, (520 mmol O₂·m^{−2} per average storm event assuming Redfield O₂:N of 137/16) if we sum daily NCP rates over a typical 15-day O₂ residence time (e.g., 150–300 mmol O₂·m^{−2}). As was the case for $\Delta O_2/Ar$ data, there is clear evidence of a decline in NCP rates during the southbound transit in 2011; the large storm that influenced the study region for most of mid-October likely resulted in some bias associated with mixing of O₂-poor water from beneath the pycnocline into the surface. However, the role of a sharply decreasing daylength—from 11 to 6 hr over the month of October—cannot be discounted. In 2012, observations of strongly negative NCP in the northern Bering/southern Chukchi region are likely similarly biased by vertical mixing in this dynamically energetic corridor.

In regions not clearly impacted by mixing bias, mean and median NCP ranged from 1 to 10 mmol O₂·m^{−2}·day^{−1} (0.8–8.3 mmol C·m^{−2}·day^{−1} if an O₂:C of 1.2 is assumed, Laws, 1991). Surprisingly, the upper end of this range is close to the POC export fluxes estimated by Lepore et al. (2007) and Moran et al. (2005) for shelf sites in the NE Chukchi during mid-summer (July–August) using a ²³⁴Th approach (13.5 ± 13 mmol C·m^{−2}·day^{−1} in 2002 and 23.5 ± 12.0 mmol C·m^{−2}·day^{−1} in 2004). Mean and ranges of NCP estimated here are within a range of mid-summer PP values previously reported in this region (70 mmol C·m^{−2}·day^{−1} average, range of 7–250 mmol C·m^{−2}·day^{−1}, based on ¹⁴C-incubations, Hill & Cota, 2005), considering that NCP typically represents a fraction of PP ranging from 0.1–0.4 (Codispoti et al., 2013).

Direct comparison to longer-term (i.e., seasonally integrated) NCP estimates calculated from nutrient or carbon inventory change is more challenging, as these estimates include high NCP associated with sea ice retreat in spring. Codispoti et al. (2013) utilized seasonal drawdown of nitrate to estimate an annual NCP for the Chukchi shelf of 5.8 mol C·m^{−2}, while Mathis et al. (2009) utilized DIC drawdown between spring and summer to calculate mean daily rates of 8–120 mmol C·m^{−2}·day^{−1}. Considering that NCP rates estimated here are from much later in the season when the community is nutrient-limited, the order of magnitude match between the range observed by Mathis et al. (2009) and that observed in October 2011 and 2012 is

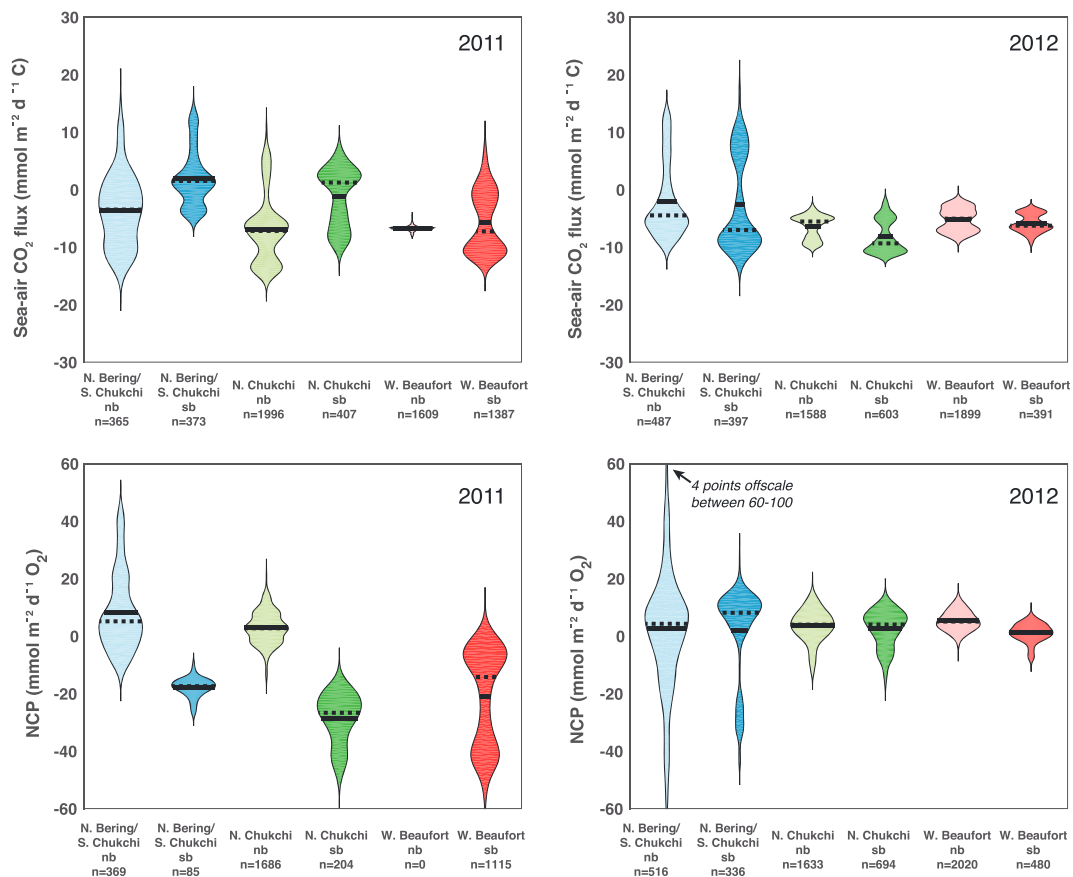


Figure 10. Violin plots indicating distributions for calculated sea-air CO₂ flux (negative values indicate invasion) and NCP in 2011 and 2012. Width of each “violin” is proportional to frequency, allowing visualization of multimodal distributions. Regions are as indicated, with “nb” and “sb” denoting northbound and southbound transits, respectively. Solid black line in each distribution indicates the mean, dashed line indicates the median. NCP = net community production.

noteworthy (Figure 10). Similarly, even the moderate NCP rates of 20 mmol C·m⁻²·day⁻¹ observed here would account for 50% of the NCP calculated from nitrate drawdown (Codispoti et al., 2013) over a 120 day (e.g., 15 June 15 to 15 October) growing season. These comparisons suggest that NCP rates estimated for this late open water timeframe are significant.

6.2. NCP and Sea-Air CO₂ Flux

Regional NCP patterns were related to observed sea-air CO₂ flux (F_{CO_2}) in ways consistent with previous discussion concerning $\Delta O_2/Ar$ and ΔpCO_2 trends. We calculated F_{CO_2} as

$$F_{CO_2} \text{ (mmol C m}^{-2} \text{ d}^{-1}\text{)} = k_{CO_2} K_o \Delta pCO_2, \quad (4)$$

where k_{CO_2} is the wind speed dependent gas transfer coefficient for CO₂ (m/day) calculated from Wanninkhof (2014), and K_o is the solubility of CO₂ (mmol·m⁻³·μatm⁻¹) calculated from Weiss (1974). Within-region variability in F_{CO_2} was similar to that observed for NCP, with the highest variability evident in the northern Bering/southern Chukchi region. Most regional averages indicated an oceanic sink for CO₂, with the exception of the northern Bering/southern Chukchi southbound survey in 2011 where outgassing was indicated. Notably, the temporal shift between northbound and southbound surveys in 2011 observed for $\Delta O_2/Ar$ and NCP is also indicated in F_{CO_2} , with a reduction of CO₂ uptake (or switch to outgassing) post-storm event.

Evans et al. (2015) recently evaluated over 580,000 surface $pCO_{2,sw}$ measurements collected throughout the Pacific Arctic and found the greatest rates of ocean CO₂ uptake on the Chukchi shelf during the late

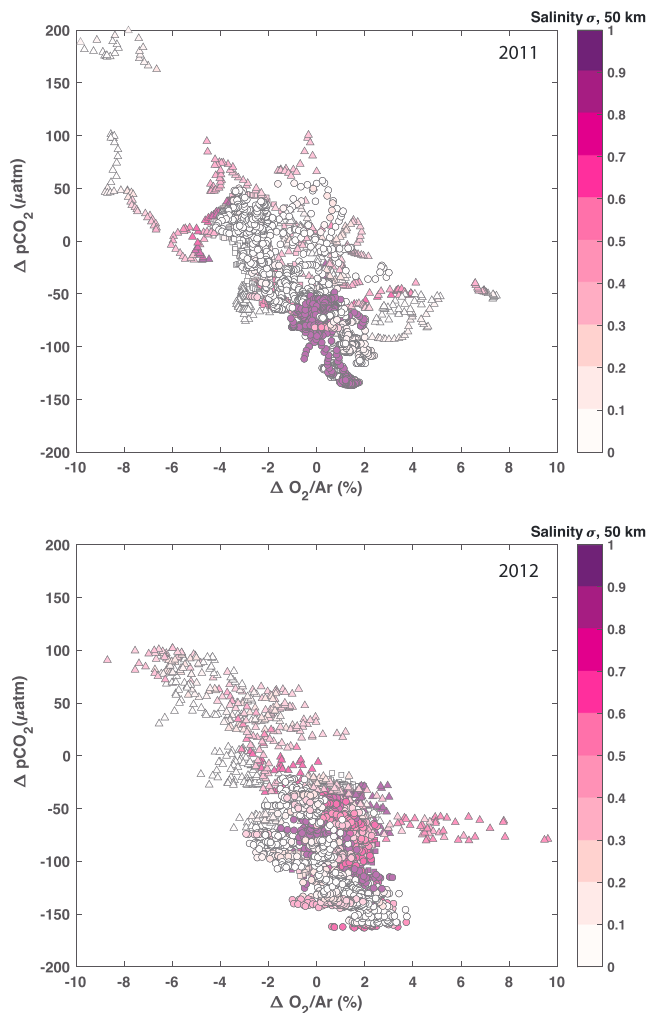


Figure 11. Relationship between $\Delta O_2/Ar$ and ΔpCO_2 , colored by variance in salinity within 50 km of each observation. Triangles, circles, and squares indicate data collected in the N. Bering/S. Chukchi, N. Chukchi, and W. Beaufort, respectively.

summer/early fall timeframe (August–October), a phenomenon attributed to large negative ΔpCO_2 , high winds, and maximal open water extent. However, ΔpCO_2 actually attain most negative values earlier in the summer (July/August), a result of intense net productivity over the shelf as sea ice retreats. Over subsequent months warming and reduced net productivity cause the ΔpCO_2 gradient to weaken slightly, and by October it is difficult to discriminate the relative contribution of the prior abiotic/biotic factors from the contribution of late season cooling and net productivity. Here our observations demonstrate that regions of maximum air-sea gradient (negative ΔpCO_2) tend to co-occur in many areas with high $\Delta O_2/Ar$ (and corresponding rates of NCP) suggesting a role for late season biological processes in determining regional CO_2 uptake.

7. Potential Mechanisms to Support a Late Open Water Season Biological CO_2 Sink

In both years, $\Delta O_2/Ar$ and ΔpCO_2 observations suggest a significant role for recent biological activity toward maintaining an ocean carbon sink in the late open water season. However, given the nitrate-deplete status of this region in this timeframe (Figures 2–5, see also Codispoti et al., 2013; Grebmeier et al., 2015; Tremblay et al., 2015), identifying the source of nutrients fueling this biologically mediated carbon sink is an obvious goal. Of particular interest is the Chukchi Sea, which had the most negative ΔpCO_2 for the late summer/early fall timeframe in the recent climatology for the Western Arctic (Evans et al., 2015) and was also found to be a strong regional sink in our observations (Figure 10).

Could storm-induced mixing play a potential role? Northeasterly winds prevailed in September–October 2011 and September 2012 (Danielson et al., 2017; Weingartner et al., 2017; Figure S1), which would favor lateral transport of nutrient-replete waters from the Beaufort basin halocline westward into Barrow Canyon (Pickart et al., 2013). Slightly elevated $[NO_3^-]$ were observed in the nearshore Chukchi and Beaufort near Barrow Canyon in both years (Figures 3 and 5), indicating this nutrient supply mechanism might help to explain elevated rates observed in the vicinity of Barrow Canyon. But how might patches of high $\Delta O_2/Ar$ and negative ΔpCO_2 on more remote areas of the outer Chukchi shelf near

Hanna Shoal be explained? Here strong stratification from MW (particularly in 2012, Weingartner et al., 2017) would presumably inhibit turbulent mixing between the surface and the nutrient-replete bottom layer. Yet recent turbulence observations from the NE Chukchi suggest that interactions of internal waves and wind-forced surface turbulence can result in higher mixing rates, even for moderate storms under strongly stratified conditions (Nishino et al., 2015; Rainville & Woodgate, 2009). The response to a moderate strength storm in this area is more likely to be small-scale and patchy, resulting from time-varying interactions at the base of the pycnocline/nutricline. Rapid consumption of this spatially variable nutrient supply by phytoplankton would potentially obscure sources and mechanisms while poor coverage of remotely sensed chlorophyll observations in this late season timeframe (Figures S7 and S8) hinders any event-scale detection from space. It is therefore difficult to attribute the observed net biological production implied from $\Delta O_2/Ar$ observations to any individual storm.

As previously discussed, Weingartner et al. (2017) found significant mesoscale variance in the surface density field in regions influenced by MW. Enhanced patchiness in density structure may hint at lateral or vertical motions that would influence coupled biophysical activity. To investigate the relationship between small-scale variance in the density field and $\Delta O_2/Ar$ and ΔpCO_2 data, we calculated S variance in spatial bins of 5, 10, 25, and 50 km using surface underway data collected within 1 day of each paired $\Delta O_2/Ar$ and ΔpCO_2 observation. Results (Figure 11, 50 km results shown, other results shown in Figure S9) suggest some

association of high $\Delta O_2/Ar$ and negative ΔpCO_2 with higher S variance at mesoscale spatial domains (>10 km) although the relationship is somewhat equivocal. This association of patchiness in physical fields with O_2 - and CO_2 -based indicators of biological activity suggests that mesoscale mechanisms of nutrient supply may be important in supporting late open water season biological carbon sequestration.

The potential influence of rare, very large storm events is also worth discussion. A strong cyclone influenced the Pacific Arctic in early August 2012 (Simmonds & Rudeva, 2012). Subsequent biophysical modeling of this event has suggested the storm significantly increased production in the Pacific Arctic sector by delivery of nutrients into surface waters of adjacent Arctic shelves, with modeled zooplankton biomass remaining elevated as late as mid-September (Zhang et al., 2014). Ship-based surveys in mid-September of that year, just prior to our own sampling, indicated surface NO_3^- depletion in the NE Chukchi, but presence of NH_4^+ in surface waters at concentrations of 0–2 μM (Danielson et al., 2017, their Figure 11), a potential indicator of continued biological activity stemming from the cyclone. Full utilization of 2 μM NH_4^+ in the ~ 1 month between the mid-September sampling by Danielson et al. (2017) and this study would increase surface O_2 saturation by 12 $\mu mol/kg$, or $\sim 3\%$ of an average surface water $[O_2] = 350 \mu mol/kg$ (assuming Redfield C:N of 6.6 and a photosynthetic quotient $\Delta O_2: -\Delta CO_2 = 1.1$ for growth supported by NH_4^+ , Laws, 1991). This signal is comparable to observed $\Delta O_2/Ar$ maxima in our observations for this region, but if it originated in mid-September (we would expect rapid utilization of any limiting nutrient), gas exchange in the month preceding our October sampling would completely eliminate any biological O_2 excess. Therefore, it is likely this region experienced multiple significant biological CO_2 sequestration events in 2012 precipitated by storms of varying magnitude.

8. Implications

The physical setting of the late open water season in the Western Arctic is changing in significant ways, with important consequences for biological carbon cycling (Ardyna et al., 2014; Pickart et al., 2013; Wassmann & Reigstad, 2011). The frequent, event-scale forcing of this region, evident in winds in each year (Figures 6, S1, and S2), highlights the need to better understand links among physical forcing, biological response, and air-sea CO_2 flux at resolutions that have not been attainable with previous biological sampling. Field-based observations of biologically regulated CO_2 uptake during this shoulder season are scarce, and ocean color coverage from passive remote-sensing platforms can be nonexistent because of clouds, daylength, and low solar angle (Behrenfeld et al., 2017); for example, MODIS 8-day average chlorophyll for September and October 2011 or 2012 indicate little usable data for this region (Figures S7 and S8). In order to make reasonable predictions of how the Pacific Arctic carbon sink will respond in the future, the mechanisms controlling CO_2 uptake in this late season timeframe must be better understood.

We have demonstrated that late season biologically mediated CO_2 uptake is a potentially significant contributor to ΔpCO_2 , the concentration gradient driving patterns of total uptake, in a strong carbon sink region of the Pacific Arctic. The importance of late season biological productivity and cooling toward maintaining large negative ΔpCO_2 at a time of maximal wind speed (and hence, gas transfer rate) has been difficult to assess with standard tools and associated limitations described above. Persistent nitrate-limitation, typically low chlorophyll, and predominance of small cells during the late open water period (Tremblay et al., 2015) contribute to a perception that the influence of biological activity is limited. Coherence in patterns of ΔpCO_2 and $\Delta O_2/Ar$ in this case is unequivocal: there is clear evidence of a biologically mediated carbon sink on the Chukchi shelf in the late open water season.

Our results have significance for future projections of Arctic Ocean CO_2 uptake. In tracking the magnitude and sign of future F_{CO_2} , it is important to distinguish that trajectories for shelf and basin net uptake are likely to be different; enhanced biological sequestration on Arctic shelves over an extended growing season could partially or completely offset a reduced uptake capacity in deep-water basins (Cai et al., 2010; Else et al., 2013) as already indicated by at least one study (Manizza et al., 2013). At the same time, increased sea ice melt and subsequent upper layer freshening will significantly increase the Revelle factor, $\left(\frac{\partial pCO_2}{\partial pCO_2} / \frac{\partial DIC}{\partial DIC} \right)$, which describes the relative increase/decrease in surface pCO_2 as a function of DIC additions and removals. DIC removal by NCP (Figure 9) would therefore have a much larger impact on pCO_2 decrease as the contribution of sea ice melt increases, enhancing the air-sea gradient which is a primary determinant

of F_{CO_2} . The Revelle factor for the Chukchi Sea already approaches a value of 19 in regions influenced by recent ice melt (see Table S1), making it nearly twice as sensitive to biological additions/removals than lower latitude sites where it is 10 or less. In addition, increasing DIC concentrations in surface waters from anthropogenic CO_2 uptake will also increase the Revelle factor (i.e., a 1% increase in DIC causes an increase of Revelle factor by about 1). This enhanced sensitivity of $pCO_{2\text{ sw}}$ to biological additions and removals of carbon necessitates quantification of the autotrophic versus heterotrophic status of Arctic shelves and basins throughout ice-free periods. Broad application of the high-resolution $\Delta O_2/Ar$ approach used here can provide this critical needed constraint.

It is also important to underscore that high-resolution $\Delta O_2/Ar$ data give unprecedented insight into intermediate time scale coupling/decoupling of circulation, mixing, and net ecosystem metabolism in this region in a manner not afforded by previous rate approaches. Prior estimates of NCP have primarily sampled two extremes of the time-space spectrum: Bottle incubation approaches sample small volumes over ~1 day time scales, and approaches based on inventory change for nutrients or inorganic carbon within a broadly defined region integrate over the entire growing season (Codispoti et al., 2013). The former approach is valuable for understanding immediate responses of phytoplankton communities to light and nutrient conditions, but containment effects, and relatively sparse sampling in space and time leads to significant scaling uncertainties. The latter approach is important for understanding seasonally integrated ecosystem activity, but the time-averaging hinders attempts to mechanistically link biological activity to important drivers on shorter time scales. Stommel (1963) wrote, “a single net does not catch fish of all sizes,” that is, we must use appropriate tools to identify processes of importance across a spectrum of spatiotemporal scales. Here we demonstrate with an intermediate-time scale tracer, O_2 , that net biological production in the late open water period is more important than previously considered.

9. Concluding Remarks

What is the impact of storms on late season biological activity and sequestration of CO_2 in the Pacific Arctic sector? This question is difficult to answer directly with the data in hand. However, features of our $\Delta O_2/Ar$ observations (mesoscale spatial variability, coupling with ΔpCO_2 , association with variance in S fields) suggest that localized and time-variable nutrient delivery mechanisms are a significant factor in this late open water period. In the context of an emerging body of literature that implicates an enhanced role for wind-driven mixing under limited ice conditions (Ardyna et al., 2014; Nishino et al., 2015; Pickart et al., 2013; Rainville & Woodgate, 2009), these $\Delta O_2/Ar$ data offer strong evidence that the late open water period is critical to understanding trajectories of Arctic ecosystems and the Arctic Ocean CO_2 sink to future change. A clear line of future research is to continue to tease apart relationships between variability in physical fields and biological productivity to better understand the role of small-scale, event-driven features in the late open water shoulder season.

We have focused discussion here on the impact of episodic processes, but large-scale, remote forcing will also undoubtedly play a role in shaping late season productivity and net metabolism in the future. This may come in the form of variable sea ice melt fractions, with associated implications for pycnocline stability or variable delivery of nutrient-rich shelf water via Bering Strait (e.g., Danielson et al., 2017; Tremblay et al., 2015). Assessing the combined impact of both local and remote forcing on Arctic ecosystems will require multiyear interdisciplinary observing efforts and research community coordination, as well as appropriate tools for resolving potential agents of change.

References

- Aagaard, K., Roach, A. T., & Schumacher, J. D. (1985). On the wind-driven variability of the flow through Bering Strait. *Journal of Geophysical Research*, 90(C4), 7213–7221. <https://doi.org/10.1029/JC090iC04p07213>
- Ardyna, M., Babin, M., Gosselin, M., Devred, E., Rainville, L., & Tremblay, J.-É. (2014). Recent Arctic Ocean sea ice loss triggers novel fall phytoplankton blooms. *Geophysical Research Letters*, 41, 6207–6212. <https://doi.org/10.1002/2014GL061047>
- Arrigo, K. R., van Dijken, G., & Pabi, S. (2008). Impact of a shrinking Arctic ice cover on marine primary production. *Geophysical Research Letters*, 35, L19603. <https://doi.org/10.1029/2008GL035028>
- Arrigo, K. R., & van Dijken, G. L. (2015). Continued increases in Arctic Ocean primary production. *Progress in Oceanography*, 136, 60–70. <https://doi.org/10.1016/j.pocean.2015.05.002>
- Ashjian, C. J., Braund, S. R., Campbell, R. G., George, J. C., Kruse, J., Maslowski, W., et al. (2010). Climate variability, oceanography, bowhead whale distribution, and Inupiat subsistence whaling near Barrow, Alaska. *Arctic*, 63(2). <https://doi.org/10.14430/arctic973>

Acknowledgments

We thank the Captain, crew, and marine technicians of the USCGC Healy for their shipboard support. We also thank anonymous reviewers for providing useful feedback that improved this manuscript. This work was supported by NSF awards 1232856 and 1504394 to L.W.J. T.T. was supported by a grant NA150AR4320064 from Climate Program Office/NOAA and R.P. by NSF PLR-1504333 and OPP-1702371. All O_2 and O_2/Ar data and metadata are available at Arcticdata.io, doi:10.18739/A21G22, and pCO_2 data are available at www.ldeo.columbia.edu/CO2 as well as from the NOAA National Centers for Environmental Information Ocean Carbon Data System at <https://www.nodc.noaa.gov/ocads/>.

- Barnhart, K. R., Miller, C. R., Overeem, I., & Kay, J. E. (2016). Mapping the future expansion of Arctic open water. *Nature Climate Change*, 6(3), 280–285. <https://doi.org/10.1038/nclimate2848>
- Bates, N. R., & Mathis, J. T. (2009). The Arctic Ocean marine carbon cycle: Evaluation of air-sea CO₂ exchanges, ocean acidification impacts and potential feedbacks. *Biogeosciences*, 6(11), 2433–2459. <https://doi.org/10.5194/bg-6-2433-2009>
- Behrenfeld, M. J., Hu, Y., O'Malley, R. T., Boss, E. S., Hostetler, C. A., Siegel, D. A., et al. (2017). Annual boom–bust cycles of polar phytoplankton biomass revealed by space-based lidar. *Nature Geoscience*, 10(2), 118–122. <https://doi.org/10.1038/ngeo2861>
- Bélanger, S., Cizmeli, S. A., Ehn, J., Matsuoka, A., Doxaran, D., Hooker, S., & Babin, M. (2013). Light absorption and partitioning in Arctic Ocean surface waters: Impact of multiyear ice melting. *Biogeosciences*, 10(10), 6433–6452. <https://doi.org/10.5194/bg-10-6433-2013>
- Cai, W.-J., Chen, L., Chen, B., Gao, Z., Lee, S. H., Chen, J., et al. (2010). Decrease in the CO₂ uptake capacity in an ice-free Arctic Ocean basin. *Science*, 329(5991), 556–559. <https://doi.org/10.1126/science.1189338>
- Carmack, E., & Wassmann, P. (2006). Food webs and physical–biological coupling on pan-Arctic shelves: Unifying concepts and comprehensive perspectives. *Progress in Oceanography*, 71(2–4), 446–477. <https://doi.org/10.1016/j.pocean.2006.10.004>
- Carmack, E. C., Yamamoto-Kawai, M., Haine, T. W. N., Bacon, S., Bluhm, B. A., Lique, C., et al. (2016). Freshwater and its role in the Arctic Marine System: Sources, disposition, storage, export, and physical and biogeochemical consequences in the Arctic and global oceans. *Journal of Geophysical Research: Biogeosciences*, 121, 675–717. <https://doi.org/10.1002/2015JG003140>
- Cassar, N., Barnett, B. A., Bender, M. L., Kaiser, J., Hamme, R. C., & Tilbrook, B. (2009). Continuous high-frequency dissolved O₂/Ar measurements by equilibrator inlet mass spectrometry. *Analytical Chemistry*, 81(5), 1855–1864. <https://doi.org/10.1021/ac802300u>
- Coachman, L. K., Aagaard, K., & Tripp, R. B. (1975). *Bering Strait: The regional physical oceanography*. Seattle: University of Washington Press.
- Codispoti, L. A., Kelly, V., Thessen, A., Matrai, P., Suttles, S., Hill, V., et al. (2013). Synthesis of primary production in the Arctic Ocean: III. Nitrate phosphate based estimates of net community production. *Progress in Oceanography*, 110, 126–150. <https://doi.org/10.1016/j.pocean.2012.11.006>
- Craig, H., & Hayward, T. (1987). Oxygen supersaturation in the ocean: Biological versus physical contributions. *Science*, 235(4785), 199–202. <https://doi.org/10.1126/science.235.4785.199>
- Danielson, S. L., Eisner, L., Ladd, C., Mordy, C., Sousa, L., & Weingartner, T. J. (2017). A comparison between late summer 2012 and 2013 water masses, macronutrients, and phytoplankton standing crops in the northern Bering and Chukchi Seas. *Deep Sea Research Part II: Topical Studies in Oceanography*, 135, 7–26. <https://doi.org/10.1016/j.dsr2.2016.05.024>
- Danielson, S. L., Weingartner, T. J., Hedstrom, K. S., Aagaard, K., Woodgate, R., Curchitser, E., & Stabenro, P. J. (2014). Coupled wind-forced controls of the Bering–Chukchi shelf circulation and the Bering Strait throughflow: Ekman transport, continental shelf waves, and variations of the Pacific–Arctic sea surface height gradient. *Progress in Oceanography*, 125, 40–61. <https://doi.org/10.1016/j.pocean.2014.04.006>
- Else, B. G. T., Galley, R. J., Lansard, B., Barber, D. G., Brown, K., Miller, L. A., et al. (2013). Further observations of a decreasing atmospheric CO₂ uptake capacity in the Canada Basin (Arctic Ocean) due to sea ice loss. *Geophysical Research Letters*, 40, 1132–1137. <https://doi.org/10.1002/grl.50268>
- Emerson, S., Ito, T., & Hamme, R. C. (2012). Argon supersaturation indicates low decadal-scale vertical mixing in the ocean thermocline. *Geophysical Research Letters*, 39, L18610. <https://doi.org/10.1029/2012GL053054>
- Evans, W., Mathis, J. T., Cross, J. N., Bates, N. R., Frey, K. E., Else, B. G. T., et al. (2015). Sea-air CO₂ exchange in the western Arctic coastal ocean. *Global Biogeochemical Cycles*, 29, 1190–1209. <https://doi.org/10.1002/2015GB005153>
- Eveleth, R., Cassar, N., Doney, S. C., Munro, D. R., & Sweeney, C. (2017). Biological and physical controls on O₂/Ar, Ar and pCO₂ variability at the Western Antarctic Peninsula and in the Drake Passage. *Deep Sea Research Part II: Topical Studies in Oceanography*, 139, 77–88. <https://doi.org/10.1016/j.dsr2.2016.05.002>
- Eveleth, R., Timmermans, M.-L., & Cassar, N. (2014). Physical and biological controls on oxygen saturation variability in the upper Arctic Ocean. *Journal of Geophysical Research: Oceans*, 119, 7420–7432. <https://doi.org/10.1002/2014JC009816>
- Garcia, H. E., & Gordon, L. I. (1992). Oxygen solubility in seawater: Better fitting equations. *Limnology and Oceanography*, 37(6), 1307–1312. <https://doi.org/10.4319/lo.1992.37.6.1307>
- Grebmeier, J. M., Bluhm, B. A., Cooper, L. W., Danielson, S. L., Arrigo, K. R., Blanchard, A. L., et al. (2015). Ecosystem characteristics and processes facilitating persistent macrobenthic biomass hotspots and associated benthivory in the Pacific Arctic. *Progress in Oceanography*, 136, 92–114. <https://doi.org/10.1016/j.pocean.2015.05.006>
- Grebmeier, J. M., Cooper, L. W., Feder, H. M., & Sirenko, B. I. (2006). Ecosystem dynamics of the Pacific-influenced northern Bering and Chukchi Seas in the Amerasian Arctic. *Progress in Oceanography*, 71(2–4), 331–361. <https://doi.org/10.1016/j.pocean.2006.10.001>
- Hamme, R. C., Cassar, N., Lance, V. P., Vaillancourt, R. D., Bender, M. L., Strutton, P. G., et al. (2012). Dissolved O₂/Ar and other methods reveal rapid changes in productivity during a Lagrangian experiment in the Southern Ocean. *Journal of Geophysical Research*, 117, C00F12. <https://doi.org/10.1029/2011JC007046>
- Hamme, R. C., & Emerson, S. R. (2002). Mechanisms controlling the global oceanic distribution of the inert gases argon, nitrogen and neon. *Geophysical Research Letters*, 29(23), 2120. <https://doi.org/10.1029/2002GL015273>
- Hamme, R. C., & Emerson, S. R. (2004). The solubility of neon, nitrogen and argon in distilled water and seawater. *Deep Sea Research Part I: Oceanographic Research Papers*, 51(11), 1517–1528. <https://doi.org/10.1016/j.dsr.2004.06.009>
- Hill, V., & Cota, G. (2005). Spatial patterns of primary production on the shelf, slope and basin of the Western Arctic in 2002. *Deep Sea Research Part II: Topical Studies in Oceanography*, 52(24–26), 3344–3354. <https://doi.org/10.1016/j.dsr2.2005.10.001>
- Juranek, L. W., & Quay, P. D. (2005). In vitro and in situ gross primary and net community production in the North Pacific Subtropical Gyre using labeled and natural abundance isotopes of dissolved O₂. *Global Biogeochemical Cycles*, 19, GB3009. <https://doi.org/10.1029/2004GB002384>
- Juranek, L. W., Quay, P. D., Feely, R. A., Lockwood, D., Karl, D. M., & Church, M. J. (2012). Biological production in the NE Pacific and its influence on air-sea CO₂ flux: Evidence from dissolved oxygen isotopes and O₂/Ar. *Journal of Geophysical Research*, 117, C05022. <https://doi.org/10.1029/2011JC007450>
- Kahru, M., Brotas, V., Manzano-Sarabia, M., & Mitchell, B. G. (2011). Are phytoplankton blooms occurring earlier in the Arctic? *Global Change Biology*, 17(4), 1733–1739. <https://doi.org/10.1111/j.1365-2486.2010.02312.x>
- Kaiser, J., Reuer, M. K., Barnett, B., & Bender, M. L. (2005). Marine productivity estimates from continuous O₂/Ar ratio measurements by membrane inlet mass spectrometry. *Geophysical Research Letters*, 32, L19605. <https://doi.org/10.1029/2005GL023459>
- Kwok, R., & Rothrock, D. A. (2009). Decline in Arctic sea ice thickness from submarine and ICESat records: 1958–2008. *Geophysical Research Letters*, 36, L15501. <https://doi.org/10.1029/2009GL039035>

- Ladd, C., Mordy, C. W., Salo, S. A., & Staben, P. J. (2016). Winter water properties and the Chukchi Polynya. *Journal of Geophysical Research: Oceans*, 121, 5516–5534. <https://doi.org/10.1002/2016JC011918>
- Laws, E. A. (1991). Photosynthetic quotients, new production and net community production in the open ocean. *Deep Sea Research Part A: Oceanographic Research Papers*, 38(1), 143–167. [https://doi.org/10.1016/0198-0149\(91\)90059-O](https://doi.org/10.1016/0198-0149(91)90059-O)
- Lepore, K., Moran, S. B., Grebmeier, J. M., Cooper, L. W., Lalande, C., Maslowski, W., et al. (2007). Seasonal and interannual changes in particulate organic carbon export and deposition in the Chukchi Sea. *Journal of Geophysical Research*, 112, C10024. <https://doi.org/10.1029/2006JC003555>
- Lowry, K. E., Pickart, R. S., Mills, M. M., Brown, Z. W., van Dijken, G. L., Bates, N. R., & Arrigo, K. R. (2015). The influence of winter water on phytoplankton blooms in the Chukchi Sea. *Deep Sea Research Part II: Topical Studies in Oceanography*, 118, 53–72. <https://doi.org/10.1016/j.dsr2.2015.06.006>
- Lu, K., Weingartner, T., Danielson, S., Winsor, P., Dobbins, E., Martini, K., & Statscewich, H. (2015). Lateral mixing across ice meltwater fronts of the Chukchi Sea shelf. *Geophysical Research Letters*, 42, 6754–6761. <https://doi.org/10.1002/2015GL064967>
- Manizza, M., Follows, M. J., Dutkiewicz, S., Menemenlis, D., Hill, C. N., & Key, R. M. (2013). Changes in the Arctic Ocean CO₂ sink (1996–2007). *Global Biogeochemical Cycles*, 27, 1108–1118. <https://doi.org/10.1002/2012GB004491>
- Mathis, J., Cross, J., Evans, W., & Doney, S. (2015). Ocean acidification in the surface waters of the Pacific-Arctic boundary regions. *Oceanography*, 25(2), 122–135. <https://doi.org/10.5670/oceanog.2015.36>
- Mathis, J. T., Bates, N. R., Hansell, D. A., & Babila, T. (2009). Net community production in the northeastern Chukchi Sea. *Deep Sea Research Part II: Topical Studies in Oceanography*, 56(17), 1213–1222. <https://doi.org/10.1016/j.dsr2.2008.10.017>
- Mathis, J. T., Pickart, R. S., Byrne, R. H., McNeil, C. L., Moore, G. W. K., Juranek, L. W., et al. (2012). Storm-induced upwelling of high pCO₂ waters onto the continental shelf of the western Arctic Ocean and implications for carbonate mineral saturation states. *Geophysical Research Letters*, 39, L07606. <https://doi.org/10.1029/2012GL051574>
- Moran, S. B., Kelly, R. P., Hagstrom, K., Smith, J. N., Grebmeier, J. M., Cooper, L. W., et al. (2005). Seasonal changes in POC export flux in the Chukchi Sea and implications for water column-benthic coupling in Arctic shelves. *Deep Sea Research Part II: Topical Studies in Oceanography*, 52(24–26), 3427–3451. <https://doi.org/10.1016/j.dsr2.2005.09.011>
- Nishino, S., Kawaguchi, Y., Inoue, J., Hirawake, T., Fujiwara, A., Futsuki, R., et al. (2015). Nutrient supply and biological response to wind-induced mixing, inertial motion, internal waves, and currents in the northern Chukchi Sea. *Journal of Geophysical Research: Oceans*, 120, 1975–1992. <https://doi.org/10.1002/2014JC010407>
- NOAA ESRL Global Monitoring Division (2016). updated annually. Atmospheric Carbon Dioxide Dry Air Mole Fractions from quasi-continuous measurements at Mauna Loa, Hawaii. Compiled by K.W. Thoning, D.R. Kitzis, and A. Crotwell. National Oceanic and Atmospheric Administration (NOAA), Earth System Research Laboratory (ESRL), Global Monitoring Division (GMD): Boulder, Colorado, USA. Version 2018-10 at <https://doi.org/10.7289/V54X55RG>
- Overland, J. E., & Wang, M. (2013). When will the summer Arctic be nearly sea ice free? *Geophysical Research Letters*, 40, 2097–2101. <https://doi.org/10.1002/grl.50316>
- Pabi, S., van Dijken, G. L., & Arrigo, K. R. (2008). Primary production in the Arctic Ocean, 1998–2006. *Journal of Geophysical Research*, 113, C08005. <https://doi.org/10.1029/2007JC004578>
- Pickart, R. S., Moore, G. W. K., Mao, C., Bahr, F., Nobre, C., & Weingartner, T. J. (2016). Circulation of winter water on the Chukchi shelf in early summer. *Deep Sea Research Part II: Topical Studies in Oceanography*, 130, 56–75. <https://doi.org/10.1016/j.dsr2.2016.05.001>
- Pickart, R. S., Nobre, C., Lin, P., Arrigo, K., Ashjian, C., Berchok, C., et al. (2019). Seasonal to Mesoscale Variability of Water Masses and Atmospheric Conditions in Barrow Canyon, Chukchi Sea, American Geophysical Union, Ocean Sciences Meeting 2016, Abstract #HE54A-1554. <http://adsabs.harvard.edu/abs/2016AGUOSHE54A1554N>
- Pickart, R. S., Schulze, L. M., Moore, G. W. K., Charette, M. A., Arrigo, K. R., van Dijken, G., & Danielson, S. L. (2013). Long-term trends of upwelling and impacts on primary productivity in the Alaskan Beaufort Sea. *Deep Sea Research Part I: Oceanographic Research Papers*, 79, 106–121. <https://doi.org/10.1016/j.dsr.2013.05.003>
- Pisareva, M., Pickart, R., Iken, K., Ershova, E., Grebmeier, J., Cooper, L., et al. (2015). The relationship between patterns of benthic Fauna and Zooplankton in the Chukchi Sea and physical forcing. *Oceanography*, 28(3), 68–83. <https://doi.org/10.5670/oceanog.2015.58>
- Quay, P. D., Peacock, C., Björkman, K., & Karl, D. M. (2010). Measuring primary production rates in the ocean: Enigmatic results between incubation and non-incubation methods at Station ALOHA. *Global Biogeochemical Cycles*, 24, GB3014. <https://doi.org/10.1029/2009GB003665>
- Rainville, L., Lee, C., & Woodgate, R. (2011). Impact of wind-driven mixing in the Arctic Ocean. *Oceanography*, 24(3), 136–145. <https://doi.org/10.5670/oceanog.2011.65>
- Rainville, L., & Woodgate, R. A. (2009). Observations of internal wave generation in the seasonally ice-free Arctic. *Geophysical Research Letters*, 36, L23604. <https://doi.org/10.1029/2009GL041291>
- Reynolds, R. W., Smith, T. M., Liu, C., Chelton, D. B., Casey, K. S., & Schlax, M. G. (2007). Daily high-resolution-blended analyses for sea surface temperature. *Journal of Climate*, 20(22), 5473–5496. <https://doi.org/10.1175/2007JCLI1824.1>
- Roach, A. T., Aagaard, K., Pease, C. H., Salo, S. A., Weingartner, T., Pavlov, V., & Kulakov, M. (1995). Direct measurements of transport and water properties through the Bering Strait. *Journal of Geophysical Research*, 100(C9), 18,443–18,457. <https://doi.org/10.1029/95JC01673>
- Rysgaard, S., Bendtsen, J., Delille, B., Dieckmann, G. S., Glud, R. N., Kennedy, H., et al. (2011). Sea ice contribution to the air–sea CO₂ exchange in the Arctic and Southern Oceans. *Tellus Series B: Chemical and Physical Meteorology*, 63(5), 823–830. <https://doi.org/10.1111/j.1600-0889.2011.00571.x>
- Sambrotto, R. N., Goering, J. J., & Mcroy, C. P. (1984). Large yearly production of phytoplankton in the Western Bering Strait. *Science*, 225(4667), 1147–1150. <https://doi.org/10.1126/science.225.4667.1147>
- Shroyer, E. L., & Pickart, R. S. (2018). Pathways, timing, and evolution of Pacific Winter Water through Barrow Canyon. *Deep Sea Research Part II: Topical Studies in Oceanography*. <https://doi.org/10.1016/j.dsr2.2018.05.004>
- Simmonds, I., & Rudeva, I. (2012). The great Arctic cyclone of August 2012. *Geophysical Research Letters*, 39, L23709. <https://doi.org/10.1029/2012GL054259>
- Stanley, R. H. R., Jenkins, W. J., Lott, D. E., & Doney, S. C. (2009). Noble gas constraints on air–sea gas exchange and bubble fluxes. *Journal of Geophysical Research*, 114, C11020. <https://doi.org/10.1029/2009JC005396>
- Stommel, H. (1963). Varieties of Oceanographic Experience. *Science*, 139(3555), 572–576.
- Sutherland, S. C., Newberger, T., & Takahashi, T. (2017). Report of underway pCO₂ measurements in surface waters and the atmosphere during June–July 2011, U. S. Coast Guard cutter Healy. Retrieved from http://www.ldeo.columbia.edu/res/pi/CO2/carbondioxide/text/CGChealy_11_2_data_report.pdf

- Takahashi, T., Sutherland, S. C., & Kozyr, A. (2017). Global ocean surface water partial pressure of CO₂ database: Measurements performed during 1957–2016 (version 2016). ORNL/CDIAC-160, NDP-088(V2015). (NCEI Accession 0160492). Version 3.3. NOAA National Centers for Environmental Information. Dataset. [accessed 9/2017]. Retrieved December 12, 2017, from https://www.nodc.noaa.gov/oceans/oceans/LDEO_Underway_Database/
- Takahashi, T., Sutherland, S. C., Chipman, D. W., Goddard, J. G., Ho, C., Newberger, T., et al. (2014). Climatological distributions of pH, pCO₂, total CO₂, alkalinity, and CaCO₃ saturation in the global surface ocean, and temporal changes at selected locations. *Marine Chemistry*, 164, 95–125. <https://doi.org/10.1016/j.marchem.2014.06.004>
- Takahashi, T., Sutherland, S. C., Sweeney, C., Poisson, A., Metz, N., Tilbrook, B., et al. (2002). Global sea–air CO₂ flux based on climatological surface ocean pCO₂, and seasonal biological and temperature effects. *Deep Sea Research Part II: Topical Studies in Oceanography*, 49(9–10), 1601–1622. [https://doi.org/10.1016/S0967-0645\(02\)00003-6](https://doi.org/10.1016/S0967-0645(02)00003-6)
- Takahashi, T., Sutherland, S. C., Wanninkhof, R., Sweeney, C., Feely, R. A., Chipman, D. W., et al. (2009). Climatological mean and decadal change in surface ocean pCO₂, and net sea–air CO₂ flux over the global oceans. *Deep Sea Research Part II: Topical Studies in Oceanography*, 56(8–10), 554–577. <https://doi.org/10.1016/j.dsr2.2008.12.009>
- Teeter, L., Hamme, R. C., Ianson, D., & Bianucci, L. (2018). Accurate estimation of net community production from O₂/Ar measurements. *Global Biogeochemical Cycles*, 32, 1163–1181. <https://doi.org/10.1029/2017GB005874>
- Top, Z., Martin, S., & Becker, P. (1985). On the dissolved surface oxygen supersaturation in the Arctic. *Geophysical Research Letters*, 12(12), 821–823. <https://doi.org/10.1029/GL012i012p00821>
- Top, Z., Martin, S., & Becker, P. (1988). A laboratory study of dissolved noble gas anomaly due to ice formation. *Geophysical Research Letters*, 15(8), 796–799. <https://doi.org/10.1029/GL015i008p00796>
- Tremblay, J.-É., Anderson, L. G., Matrai, P., Coupel, P., Bélanger, S., Michel, C., & Reigstad, M. (2015). Global and regional drivers of nutrient supply, primary production and CO₂ drawdown in the changing Arctic Ocean. *Progress in Oceanography*, 139, 171–196. <https://doi.org/10.1016/j.pocean.2015.08.009>
- Walsh, J. J., Dieterle, D. A., Muller-Karger, F. E., Aagaard, K., Roach, A. T., Whitledge, T. E., & Stockwell, D. (1997). CO₂ cycling in the coastal ocean. II. Seasonal organic loading of the Arctic Ocean from source waters in the Bering Sea. *Continental Shelf Research*, 17(1), 1–36. [https://doi.org/10.1016/0278-4343\(96\)00021-0](https://doi.org/10.1016/0278-4343(96)00021-0)
- Wanninkhof, R. (2014). Relationship between wind speed and gas exchange over the ocean revisited: Gas exchange and wind speed over the ocean. *Limnology and Oceanography: Methods*, 12(6), 351–362. <https://doi.org/10.4319/lom.2014.12.351>
- Wassmann, P., & Reigstad, M. (2011). Future Arctic Ocean seasonal ice zones and implications for pelagic-benthic coupling. *Oceanography*, 24(3), 220–231. <https://doi.org/10.5670/oceanog.2011.74>
- Weingartner, T., Fang, Y.-C., Winsor, P., Dobbins, E., Potter, R., Statscewich, H., et al. (2017). The summer hydrographic structure of the Hanna Shoal region on the northeastern Chukchi Sea shelf: 2011–2013. *Deep Sea Research Part II: Topical Studies in Oceanography*, 144, 6–20. <https://doi.org/10.1016/j.dsr2.2017.08.006>
- Weiss, R. F. (1974). Carbon dioxide in water and seawater: The solubility of a non-ideal gas. *Marine Chemistry*, 2(3), 203–215. [https://doi.org/10.1016/0304-4203\(74\)90015-2](https://doi.org/10.1016/0304-4203(74)90015-2)
- Woodgate, R., Stafford, K., & Prah, F. (2015). A synthesis of year-round interdisciplinary mooring measurements in the Bering Strait (1990–2014) and the RUSALCA years (2004–2011). *Oceanography*, 28(3), 46–67. <https://doi.org/10.5670/oceanog.2015.57>
- Woodgate, R. A., Weingartner, T. J., & Lindsay, R. (2012). Observed increases in Bering Strait oceanic fluxes from the Pacific to the Arctic from 2001 to 2011 and their impacts on the Arctic Ocean water column. *Geophysical Research Letters*, 39, L24603. <https://doi.org/10.1029/2012GL054092>
- Zhang, J., Ashjian, C., Campbell, R., Hill, V., Spitz, Y. H., & Steele, M. (2014). The great 2012 Arctic Ocean summer cyclone enhanced biological productivity on the shelves. *Journal of Geophysical Research: Oceans*, 119, 297–312. <https://doi.org/10.1002/2013JC009301>